A Study on Range Cell Migration Correction in SAR Imagery and MATLAB Implementation of Algorithms

Anup Parashar
Roll no. 213EC6265

Department of Electronics and Communication Engineering
National Institute of Technology, Rourkela
Rourkela, Odisha, India
June, 2015

A Study on Range Cell Migration Correction in SAR Imagery and MATLAB Implementation of Algorithms

Thesis submitted in partial fulfillment of the requirements for the degree of

Master of Technology

in

Signal and Image Processing

by

Anup Parashar

Roll no. 213EC6265

under the guidance of

Dr. Lakshi Prosad Roy

Department of Electronics and Communication Engineering

National Institute of Technology, Rourkela

Rourkela, Odisha, India

June, 2015

dedicated to my parents...

National Institute of Technology
Rourkela

DECLARATION

I declare that

1. The work contained in the thesis is original and has been done by myself under the supervision of my supervisor.
2. The work has not been submitted to any other Institute for any degree or diploma.
3. I have followed the guidelines provided by the Institute in writing the thesis.
4. Whenever I have used materials (data, theoretical analysis, and text) from other sources, I have given due credit to them by citing them in the text of the thesis and giving their details in the references.
5. Whenever I have quoted written materials from other sources, I have put them under quotation marks and given due credit to the sources by citing them and giving required details in the references.

Anup Parashar

National Institute of Technology
Rourkela

CERTIFICATE

This is to certify that the work in the thesis entitled "**A Study on Range Cell Migration Correction in SAR Imagery and MATLAB Implementation of Al-gorithm**" submitted by ***Anup Parashar*** is a record of an original research work carried out by him under my supervision and guidance in partial fulfillment of the requirements for the award of the degree of Master of Technology in Electronics and Communication Engineering (Signal and Image Processing), National Institute of Technology, Rourkela. Neither this thesis nor any part of it, to the best of my knowledge, has been submitted for any degree or academic award elsewhere.

Dr. Lakshi Prosad Roy
Assistant Professor
Department of ECE
National Institute of Technology
Rourkela

Acknowledgment

This work is one of the most important achievements of my career. Completion of my project would not have been possible without the help of many people, who have constantly helped me with their full support for which I am highly thankful to them.

First of all, I would like to express my gratitude to my supervisor **Dr. Lakshi Prosad Roy** , who has been the guiding force behind this work. I want to thank him for giving me the opportunity to work under him. He is not only a good Professor with deep vision but also a very kind person. I consider it my good fortune to have got an opportunity to work with such a wonderful person.

I am also very obliged to **Prof. K.K. Mahapatra**, HOD, Department of Electronics and Communication Engineering for creating an environment of study and research. I am also thankful to Prof. A.K Swain, Prof. A.K. Sahoo Prof. S. Meher, Prof. S. Maiti, Prof. D.P. Acharya and Prof. S. Ari for helping me how to learn. They have been great sources of inspiration.

Anup Parashar

Abstract

Synthetic Aperture Radar(SAR) is an active microwave remote sensing technology that is used to create two-dimensional images of targets and the Earth surface through the use of radar [16]. SAR has many real time applications in different fields like as hydrology, geophysics, archeology etc. The term synthetic in the name comes from the concept of effectively creating a very long, narrow antenna by post-processing signal analysis rather than using a physical structure. This yields a much better resolution in the axis perpendicular to the radar beam(called the azimuth axis) effectively yielding images with quality normally only possible by using a much larger physical radar antenna.
Goal of this thesis is to study and implementation of range doppler algorithm in MATLAB to extract out focused Single Look Complex (SLC) image that can be used for Automatic Target Recognition (ATR) and different techniques to correct range cell migration. The simulation results presented in this thesis are obtained from MATLAB environment where it is implemented a two-dimension SAR target space as originally introduced by Brain Zaharris[22]. In this thesis, we have first implemented Range Doppler Algorithm(RDA) using synthetic data to get SLC image. Then RDA is used for the formation of SLC image from practical SAR data. In the simulation results, RDA has been implemented using SAR raw data that is collected from European Space Agency (ESA) via David Sandwell's Data [13].

For focusing a moving target we need velocity compensation techniques. When the velocity of target is known by some other sources then range shifting methods will give good result for the focusing of moving target. However, this method will give good results only for a single moving target. For analysis of multiple moving target Keystone transformation (that is nothing but scaling of slow time parameter for uncoupling of fast frequency and slow time) will give better results. Keystone formatting [11] has the capability of compensating multiple targets range walk simultaneously without using any specific knowledge of the target motion, so it is widely used in the imaging of ground

moving target[10] and dim target detection area [23].Therefore also, we have considered different relative velocity of targets with respect to SAR. Then range doppler matrix is formed and analyze the effect on moving target when velocity get increased.

Keywords: RADAR, SAR, Range Doppler Algorithm, Keystone Transformation, Doppler Effects

Contents

Declaration **iv**

Certificate **v**

Acknowledgment **vi**

Abstract **vii**

List of Figures **xi**

1 Thesis overview **2**
- 1.1 SAR Imaging Principle 2
- 1.2 Problems observed in SAR imaging system 3
- 1.3 Motivation 4
- 1.4 Objective 5
- 1.5 Thesis Organization 5

2 Introduction **8**
- 2.1 RADAR 8
- 2.2 Synthetic Aperture Radar 9
- 2.3 Synthetic Aperture Radar Platform 9
- 2.4 SAR Transmit Pulse 11
- 2.5 SAR Receive Pulse 12

3 The Range Doppler Algorithm(RDA) For SAR Raw Data Image Formation **18**
- 3.1 The Range Doppler Algorithm 18

3.1.1 Range Compressed Signal 19
3.1.2 Range Doppler Signal 20
3.1.3 Final Processed SAR Image 21
3.2 Two-Dimensional SAR Imaging through Simulation 21
3.2.1 Range Cell Migration 24

4 The Keystone Transformation for Correcting Range Cell Migration 30
4.1 Introduction 30
4.2 Problem 30
4.3 Compensation by Range Shifting 35
4.4 The Keystone transformation 37

5 Implimentation of Existing Methods in MATLAB 44
5.1 Simulation results obtained by RDA 44
5.2 Simulation Results Obtained On Correction of RCMC using Keystone Transformation Method 49

6 Conclusion and Future Work 52
6.1 Conclusion 52
6.2 Future work 52

Bibliography 53

List of Figures

1.1 Basic block diagram of SAR system 2

2.1 Synthetic Aperture Radar Modes 10
2.2 Effect of Pulse Repetition Interval on Transmit and Receive Pulse 12
2.3 Received signal strength vs. sensor position 14
2.4 Squint Angle Geometry 15
2.5 SAR Data Storage in Memory 16

3.1 RDA Block Diagram 19
3.2 Radar Range Finding Matched Filter Example 20
3.3 Raw SAR Signal Space 22
3.4 Zoomed in Center Raw SAR Signal Space 23
3.5 Range Reference Signal 23
3.6 Range Cell Migration 24
3.7 Range Time Signal at Center Azimuth Compression Example . 25
3.8 Range Compressed Image 26
3.9 Image of range compressed signal 27
3.10 Image after RCMC 27
3.11 Final Processed SAR Image of Single Point Target 28

4.1 Range-Doppler matrix for a single target without range migration. Arrangement of fasttime/ slow-time data. Resulting range-Doppler matrix 31
4.2 Range-Doppler matrix with no range migration.(a)Range vs. pulse number. (b)Zoom into the central portion of the resulting range-Doppler matrix. 34

4.3 Range-Doppler matrix with range migration(a)Range vs. pulse number.(b)Zoom into non-zero portion of the resulting range-Doppler matrix. 35
4.4 Range-Doppler matrix with range migration and compensation using DFT phase multiplies. Compare to the spectrum shape in Figs. 2 and 3. (a) Range vs. pulse number.(b)Zoom into non-zero portion of the resulting range-Doppler matrix. 36
4.5 Range-Doppler matrix with range migration and compensation using the keystone transformation. Compare to Figs. 4.3 and 4.4. (a) Range vs. pulse number. (b) Zoom into non-zero portion of the resulting range-Doppler matrix. 41
4.6 Range-Doppler matrix with multiple targets at different velocities. (a) Range vs. pulse number. (b) Zoom into non-zero portion of the resulting range-Doppler matrix. 41
4.7 Result of applying the keystone transformation to example of Fig. 6. (a) Range vs. pulse number. (b) Zoom into non-zero portion of the resulting range-Doppler matrix. 42

5.1 (a) Echo geenrated by targets. (b) Reference signal in range time domain. (c) Reference signal in frequency domain. (d) Range cell migration compensation output 44
5.2 Range Compressed Image 45
5.3 Image After RCMC 46
5.4 The final SAR image generated from the two dimensional simulation of a single point target 46
5.5 Raw Image 47
5.6 Range compressed image of first patch 48
5.7 Single Look Complex Image 49
5.8 Range-Doppler matrix with no range migration.(a)Range vs. pulse number. (b)Zoom into the central portion of the resulting range-Doppler matrix. 49

5.9 Range-Doppler matrix with range migration(a)Range vs. pulse number.(b)Zoom into non-zero portion of the resulting range-Doppler matrix. 50
5.10 Range-Doppler matrix with range migration and compensation using DFT phase multiplies. Compare to the spectrum shape in Figs. 2 and 3. (a) Range vs. pulse number.(b)Zoom into non-zero portion of the resulting range-Doppler matrix. 50
5.11 Range-Doppler matrix with range migration and compensation using the keystone transformation. Compare to Figs. 3 and 4. (a) Range vs. pulse number. (b) Zoom into non-zero portion of the resulting range-Doppler matrix. 51
5.12 Range-Doppler matrix with range migration and compensation using the keystone transformation. Compare to Figs. 3 and 4. (a) Range vs. pulse number. (b) Zoom into non-zero portion of the resulting range-Doppler matrix. 51

Chapter 1

Thesis Overview

SAR Imaging Principle

Motivation

Objective

Thesis Organization

Chapter 1

Thesis overview

1.1 SAR Imaging Principle

Synthetic aperture radar is a such type of Radar that is similar to a conventional radar mounted on spacecraft (moving platform), in which sequentially transmitted electromagnetic (EM) waves having specific Pulse Repetition Frequency (PRF) backscattered from earth surface and radar antenna collect echo signal with the help of receiver section. In SAR consecutive transmission and reception with appropriate coherent combination make a virtual aperture which is larger than actual antenna length [6, 8]. SAR system block diagram is shown

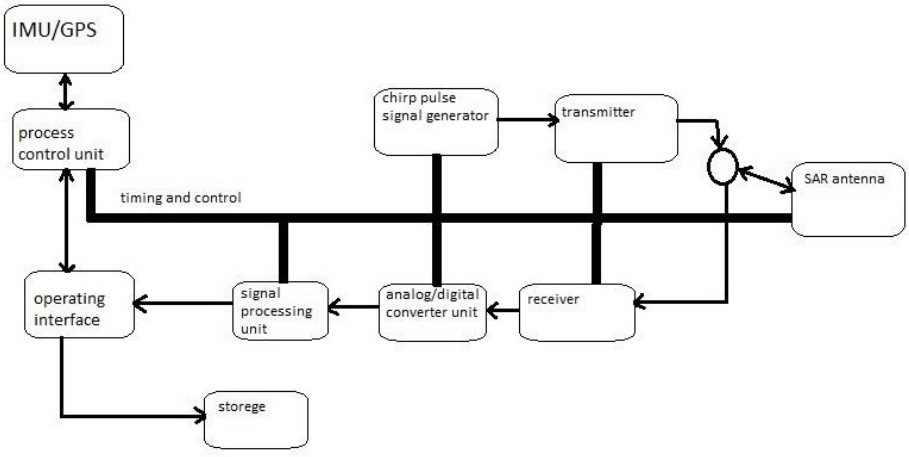

Figure 1.1: Basic block diagram of SAR system

in figure 1.1 in which processor control unit generates timing and control signals. Chirp pulse signal generator generate Stepped frequency or liner fre-

quency modulated pulse. In the above SAR system block contains single antenna for transmission and reception. First transmitter transmit radar pulse to the targets or seen,after that reflected signal is collected(received) at receiver mounted on SAR antenna. Once receiver gets echo signal then it passes signal to analog to digital converter(ADC) for further processing. ADC unit is then sampled and quantized the received signal.

This digital signal is then passed through signal processing unit, Last unit signal is nothing but raw SAR signal that contain errors occurred due to movement of platform and others effect. Error occur due to the relative movement of platform and targets is also know as Range cell Migration (RCM). Other correction such as Range walk correction, atmospheric effect, speckle noise removal has to be done on SAR raw signal.

1.2 Problems observed in SAR imaging system

During processing of raw sar data for imaging purpose, some problems comes into picture. Some of them can be easily removable but some are quit serious and need complex processing to overcome from the error occurred at the time of formation of raw data. Few of them are given below.

Range migration

Due to the movement of platform, Range of stationary target change during Coherent Processing Interval(CPI), and make target range change. Range distance follow hyperbolic curve for the stationary target that should be compensated. This hyperbolic curve is also known as range curvature. Due to change in the range of stationary target, range cell migrates to the another cells. This phenomena is know as range migration[6, 8]. Another range migration is due to range walk effect. This phenomena occur if CPI is more, then revolution of earth makes shifting in the position of object/targets with respect to SAR platform. Doppler effect is unique signature for the relative movement. So to correct range cell migration, doppler frequency domain procedure will give good result.

If the range error comes after these effects is δR. so, Total range can be

written as $R+\delta R$ is equal to

$$R+\delta R=\left(R^2+\left(\frac{v_y T_s}{2}\right)^2\right)^{\frac{1}{2}} \tag{1.1}$$

So we have, $T_s=\frac{R\Omega}{v_y}$, using above expression we can calculate R in form of R and

$$\delta R=R\frac{\Omega^2}{8} \tag{1.2}$$

with $\Delta r=$ resolution

$$N=\frac{\delta R}{\Delta r}=R\frac{\Omega^2}{8\Delta r} \tag{1.3}$$

Now, if N is more than 1, range migration has to be corrected , if N is less than 1, there is no need for the correction of RCM.

Motion errors in SAR imaging

The SAR basic theory is based on the assumption that the desired target is stationary. If a target is moving doppler shift posed due to the velocity of target gives wrong distance information about the position of the object followed to phase of the received electromagnetic waves [6, 8]. When moving target's speed is very high, it covers the several pixels of image during the Coherence Integration Interval(CPI) of SAR. Due to this image formed without correction of RCM is smeared in both azimuth and range direction. When the speed is very low then it does cross other pixel during CPI and hence no need of RCM required at this time.Different type of motion compensation techniques are available to rectify above problem in the thesis.

1.3 Motivation

SAR imagery is mainly used for Automatic Target Recognition(ATR), oceanology, mine detection, ecology, remote sensing, geology, archeology etc. Major problem occurs in SAR imagery is that range cell migration has to be corrected for further processing of SAR raw data. We have different methods to compensate range cell migration. Some of these technique to correct RCM are range

shifting method , Keystone transformation methods. Keystone transformation method is newest and very efficient method for the correction of range cell migration. Due to operated in range doppler domain it is more efficient and fast as compared to other domain.

1.4 Objective

To remove range cell migration problem in SAR imagery, first of all we need to process raw SAR data using some algorithm such as Range Doppler Algorithm(RDA), Omega-K Algorithm. In this thesis we successfully implemented RDA algorithm that change raw SAR data to Single Look Complex(SLC) image. In mid of algorithm(Range Doppler domain), we will apply different methods for the correction of range cell migration(RCM). We create two scenario as follow.

First one is when platform is moving but target is not moving. In this scenario RCM correction can be easily done by proper adjustment of range migration in CPI duration. Image formed after applying RDA is nothing but compressed in both azimuth and range to know exact co-ordinate of the targets.
In second scenario, targets have some velocity that also take some contribution for range cell migration. In this scenario, we assume relative velocity of target v with respect to SAR platform. Keystone transformation method is used for the correction of range cell migration.

1.5 Thesis Organization

This thesis is organized into six chapters.
The first chapter deals with the basics SAR imaging and problem regarding SAR imaging.
Chapter 2 deals with how SAR transmits and receive data and its parameters.
Chapter 3 deals The Range Doppler Algorithm(RDA) For SAR Raw Data Image Formation.
Chapter 4 contains The Keystone Transformation for Correcting range cell migration.

Chapter 5 deals with simulation results for both RDA algorithm used for imaging pupose and correction of range cell migration using keystone transformation.
In chapter 6 , conclusion and future work is given.

Chapter 2

Introduction

RADAR

Synthetic Aperture Radar

Synthetic Aperture Radar Plateform

SAR Transmit Pulse

SAR Receive Pulse

Chapter 2

Introduction

2.1 RADAR

In synthetic aperture radar (SAR) imaging, microwave pulses (electromagnetic waves) are transmitted by an antenna towards the earth surface. The microwave energy(EM wave) scattered back to the spacecraft is then calculated . The SAR imaging technique is similar to radar principle to form an image by utilizing the time delay of the backscattered signals. SAR is used in many military and civilian applications. The pulse transmitted by SAR antenna is get reflected back from the targets. The receiver collects all the echoes comes from targets and clutter. the returning waves(echoes) is then processed via receiver. According to the properties of returning pulse, which get received at the receiver and further processed, information is being extracted out such as distance of the desire target, velocity of the targets, shape and size of the targets etc. All these information is extracted from the properties of transmitted and received pulse such as propagation delay, reflectivity factor, doppler phenomena etc[17]. Radar transmitter allows for detection that is independent on the external sources for the illumination purpose of target space, But in others detection system, they mostly depends on illumination from sun or other light sources that restrict their application in the absence of these sources (in absence of light). Due to these advantages, radar is used in many remote sensing applications in the civilian and military sectors[18]. The Synthetic Aperture Radar (SAR) technique is used to increase the resolution of radar systems. In SAR processing, multiple

scatterers signals are stored in the form of array as station moves across the target area. Assuming Platform velocity is constant then using range and azimuth information collected by the retuning pulse , higher resolution can be achieved.

2.2 Synthetic Aperture Radar

The realization of Synthetic Aperture Radar (SAR) is often credited to Carl Wiley of Goodyear Aerospace in 1951. SAR is an active microwave remote sensing technology that is used to create two-dimensional images of targets and the Earths surface through the use of radar [16]. The term synthetic in the name comes from the concept of effectively creating a very long, narrow antenna by post-processing signal analysis rather than using a physical structure. This yields a much better resolution in the axis perpendicular to the radar beam (called the azimuth axis) effectively yielding images with quality normally only possible by using a much larger physical radar antenna [21].

SAR became an important aspect of remote sensing in the 1970s when SAR technology was introduced to satellite platforms [13]. The further increase in the use of SAR is based mostly on the following principles: radar requires no illumination and works well in darkness, the electromagnetic waves of radar frequencies pass through clouds with very minimal deterioration, and radar scatters off targets much differently than optical energy, allowing for a different perspective of surfaces than optical sensors can provide.

2.3 Synthetic Aperture Radar Platform

There are only two direction of interest namely azimuth and range where azimuth direction is parallel to the motion of the radar platform, and it is also known as the slow time direction. The name slow comes due to relatively slow velocity of of radar platform with respect to pulse velocity . The range direction is oriented orthogonal to the platform motion, and parallel to the beam direction. This direction is also referred to as the fast time, as this is the direction that the radar pulses are transmitted. As the platforms moves in the azimuth direction, multiple radar pulses are sent along the range direction. For each radar

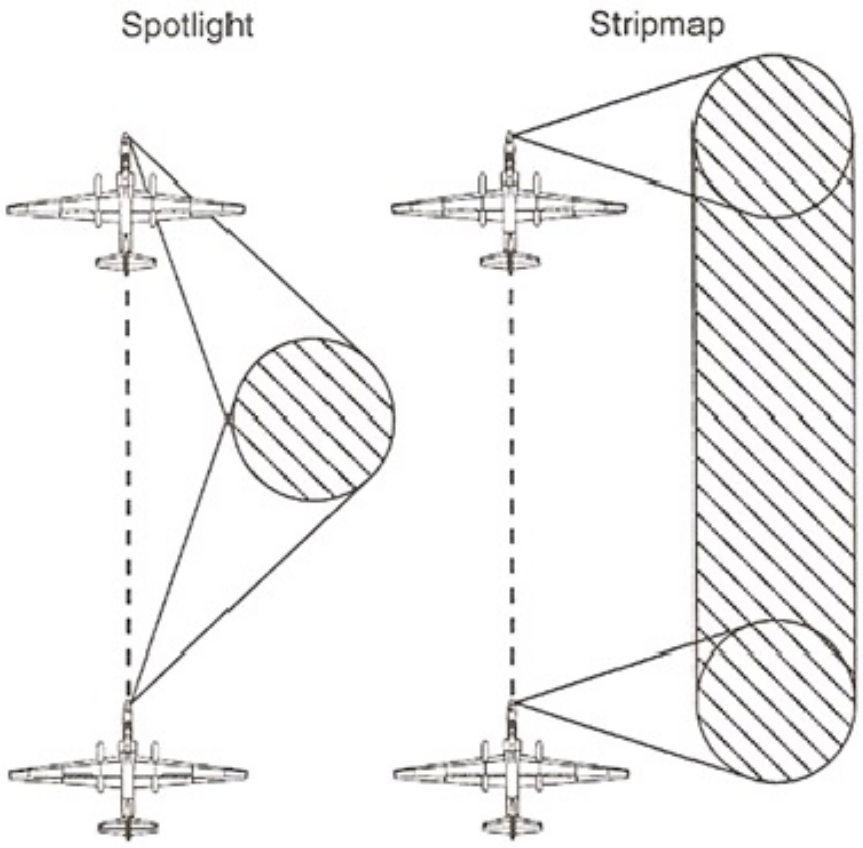

Figure 2.1: Synthetic Aperture Radar Modes

pulse sent out, a certain area in the target space is illuminated and contributes to the radar return. This area is known as the footprint, and is the part of the target space that radiates signal back to the receiver. In the strip-map mode of SAR, the pulses are always orthogonal to the direction of travel. Subsequently, the radar pulses cover each area in the target space for an equal amount of time. Alternatively, the radar can be configured to point towards a certain area continuously as the platform moves across the target space. This technique is called spotlight mode, analogous to a spotlight being focused at a target [18]. Since the radar is continuously focused on one location instead of sweeping a target area orthogonally, spotlight mode results in more radar returns from the target in question, but at the expense of the total area covered by the radar returns. The simulation environment used for this thesis uses the strip-map SAR mode. The two modes are shown in Figure 2.1. As the platform moves across the tar-

get space, the distance between the radar transmitter and the target of interest continually changes. This distance is called the slant range, and is an important parameter for calculating the Doppler shift the radar pulses experience at each transmission location. The squint angle is closely related, which is the angle that the slant range makes with the zero Doppler shift plane; that is, the range that results in no Doppler shift. The squint angle and slant range are important parameters in the calculations for the Doppler shift of the platform that are used to combine the multiple radar returns into a single image. In addition to distance variables, there are time variables that are used in SAR calculations. Fast time is the time variable for the speed of the radar pulses. Slow time is the time variable used for the velocity of the platform. These variables will be used later in the derivation of the SAR signal. The SAR pulsed radar operates on a series of transmit and receive cycles. The echoes received by the radar are aggregated and used to compute the SAR signal space. Each of the two stages will be discussed at length.

2.4 SAR Transmit Pulse

During SAR radar operation, a frequency-modulated signal is transmitted by the radar. The signal is characterized by Equation 2.1

$$s_{pul}(t) = w_r(t)cos(2\pi f_c t + \pi k_r t^2) \tag{2.1}$$

$w_r(t)$ =Rectangular function representing pulse duration in fast time
f_c =Carrier frequency
k_r = Chirp Rate

The term $\pi k_r t^2$introduces a chirp in the transmitted signal, which causes a linear change in frequency as a function of fast time. A positive value of K_r is referred to an up chirp, while a negative value is referred to as a down chirp. The inclusion of an up chirp or a down chirp improves the accuracy of the range information, since the received frequency can be used to determine exactly when the pulse reached the target. The individual parameters will be discussed further in subsequent sections.

Other important values used in SAR are the signal bandwidth, B_0, chirp

pulse duration,t_r, and the range resolution, rho_r. Equations 2.2 and 2.3 describe the relationships between the variables.

$$B_0 = |k_r| t_r) \tag{2.2}$$

$$\rho_r = \frac{c}{2B_0} \tag{2.3}$$

c = speed of light
Each frequency-modulated signal is transmitted at a specified frequency, known as the Pulse Repetition Frequency (PRF). The inverse of the PRF is called the Pulse Repetition Interval. Figure 2.2 illustrates the transmit and receive sequence of a SAR signal. As can be seen, there is a linear increase in frequency

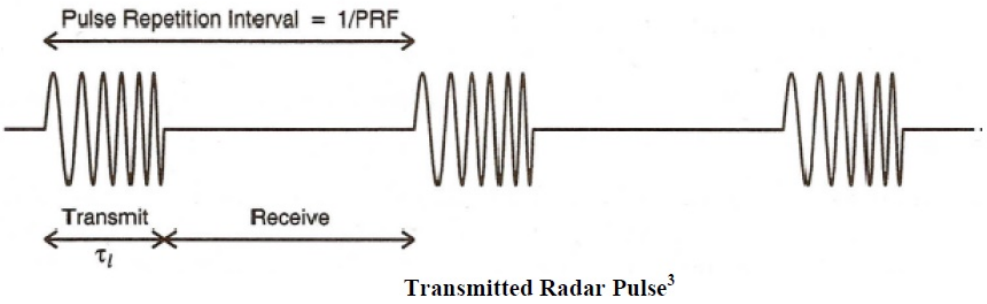

Figure 2.2: Effect of Pulse Repetition Interval on Transmit and Receive Pulse

of the transmit pulse. This is due to an up chirp added to the signal

2.5 SAR Receive Pulse

Once the SAR signal has been transmitted, the system listens for the received signal. A single received signal can be represented as shown in Equation 2.4.

$$s_r(t) = F_n * w_r(t - \frac{2R_0}{c}) e^{-j(4\pi \frac{f_c R_0}{c} + \pi k_r (t - \frac{2R_0}{c})^2)} \tag{2.4}$$

R_0 = range at zero slant angle
F_n = reflectivity of target
c= speed of light
f_c= carrier frequency

The received signal is proportional to the reflectivity of the target, as well as the flight time of the signal from the transmitter and then to the receiver. The total time is twice the instantaneous slant range to the target, divided by the speed of light. The received signal is complex and with both a baseband and high frequency carrier terms since the signal has been quadrature modulated. The high frequency carrier term will be removed. As the radar platform moves through the target space, there are additional factors that need to be considered to characterize the received signal. The movement in the azimuth direction, or slow time, affects both the slant range and the amplitude of the signal. In this paper, the platform is assumed to be moving at a constant velocity in the azimuth direction, and in azimuth and range distances small enough that there is a clear line of sight from the platform to all points in the target space. The equation for the instantaneous slant range as a function of slow time is shown as Equation 2.5.

$$R(\eta) = \sqrt{R^2{}_0 + V^2{}_r \eta^2} \tag{2.5}$$

R_0 = range at zero slant angle
V_r = velocity of radar platform
η = slow time

The slow time,η , is considered to be negative before the platform reaches zero slant angle and positive as the platform moves away. As Figure 2.3 shows, the distance of closest approach is achieved when the slant angle is zero[**?**]

In addition to the slant range, the amplitude of the received signal is also affected by the slow time. As shown in Figure 2.3, the strongest return occurs when the center of the beam pattern is on the target. The small side lobes also produce small peaks where the return is strong. When the target first enters the target space, the platform is moving towards the target, and so the Doppler frequency shift is positive. This case is shown in sensor position A, when the target is entering the main lobe of the signal. When the target is situated in the middle of the bin (sensor position B), the relative velocity between the platform and the target is zero, so there is no frequency shift. As the platform continues moving, the Doppler shift becomes increasingly negative. This situation is shown in position C. The target has passed from the main lobe of the system.

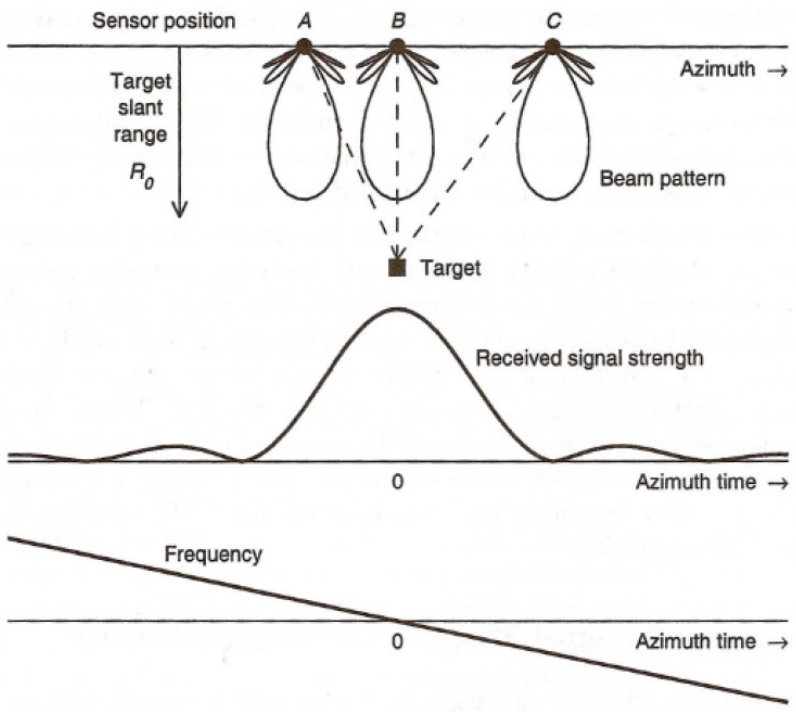

Azimuth Beam Pattern[3]

Figure 2.3: Received signal strength vs. sensor position

However, the transmitted signal has small side lobes that contribute some energy, so the received signal has small side lobes as well[3].
Equation 2.6 shows the amplitude of the received signal as a function of slow time

$$w_a(\eta) \approx \rho^2{}_a\{\theta(\eta)\} \approx sinc^2(\frac{0.886\theta(\eta)}{\beta_{bw}}) \tag{2.6}$$

Due to the propagation of the signal in both directions, the returning beam pattern is approximated by a $sinc^2$ function, and is expressed as a function of . The variations in the instantaneous slant range and amplitude result in the modified received signal equation, which is shown as Equation 2.7.

$$s_r(t,\eta) = F_n * w_r(t - \frac{2R(\eta)}{c}) w_a(\eta - \eta_c) e^{-j(4\pi\frac{f_c R\eta}{c} + \pi k_r (t - \frac{2R\eta}{c})^2)} \tag{2.7}$$

The equation for the Doppler bandwidth of the SAR system is shown as Equation 2.8.

$$\Delta f_{dop} = \frac{2V_s \cos\theta_{sq}}{\lambda}\theta_{bw} \tag{2.8}$$

The Doppler bandwidth is an important quantity, as is affects the minimum sampling rate needed in the azimuth resolution. According to the Nyquist theorem, the SAR sampling rate in the azimuth resolution must meet or exceed the Doppler bandwidth to avoid aliasing of the signal.

The squint angle is represented by ,θ_{sq}, and is the angle between the zero Doppler plane and the vector from the platform to the target. The squint angle is shown in Figure 2.4. The squint angle is a function of the location of the

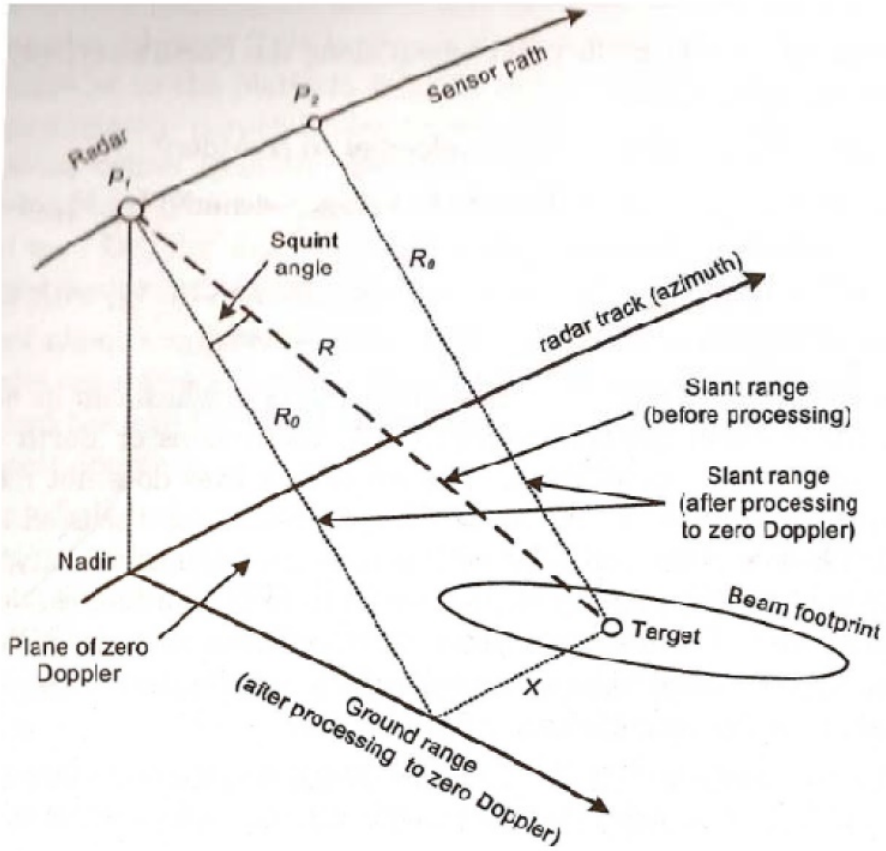

Figure 2.4: Squint Angle Geometry

platform, and subsequently is dependent on the azimuth time of the system.

The equation for the squint angle is shown as Equation 2.9.

$$\theta_{sq} = \cos^{-1}\left(\frac{R_{0_m}}{R_m(\eta)}\right) \tag{2.9}$$

It decreases as the platform approaches the target, reaches zero when the platform is at its closest position to the target, and increases as the platform continues past the target.Each of the received signals is stored in a two-dimensional array, as shown in Figure 2.5. Each signal is added into the array as it is re-

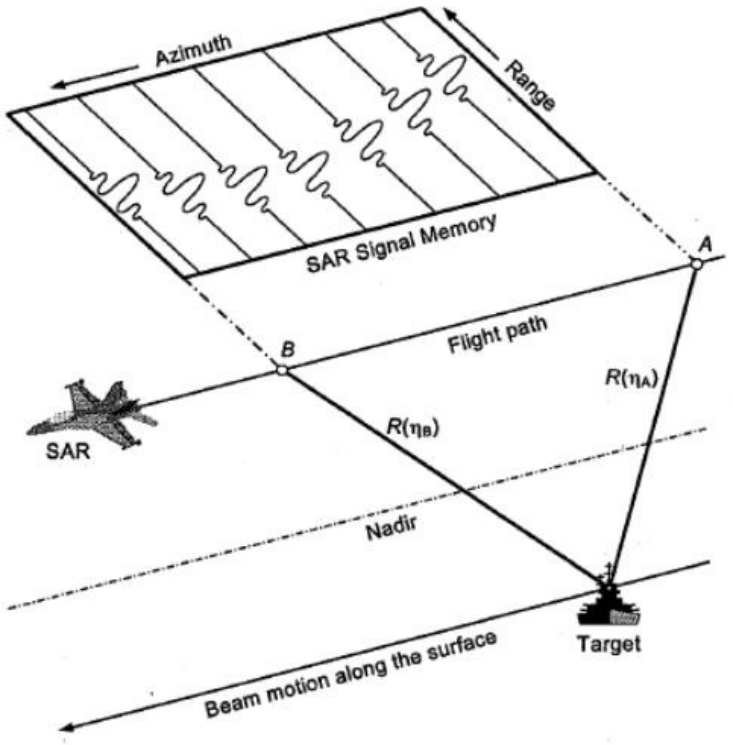

Figure 2.5: SAR Data Storage in Memory

ceived, and each point of the signal is stored horizontally. This orders the data such that each row represents the entirety of a single received signal, and each column is the data received from a particular range distance[16, 3].

Chapter 3

The Range Doppler Algorithm(RDA) For SAR Raw Data Image Formation

The Range Doppler Algorithm
Two-Dimensional SAR Imaging through Simulation

Chapter 3

The Range Doppler Algorithm(RDA) For SAR Raw Data Image Formation

3.1 The Range Doppler Algorithm

The Range Doppler algorithm[3, 16] is a widely used Synthetic Aperture Radar processing technique that utilizes match filtering to generate high-resolution images of targets. Range Doppler processing is very efficient because the match filtering process can be done entirely in the frequency domain. The convolution operations that would be necessary in the time domain can therefore be replaced by multiplication operations, greatly increasing processing speed. In addition, the entire target space is processed at once, allowing all targets to be processed simultaneously with a single set of operations. The name Range Doppler stems from a particular step in the process, when the target space data in the azimuth, or Doppler, direction is represented in the frequency domain, and the range data has already been compressed. The steps involved in the Range Doppler are detailed in the following sections.

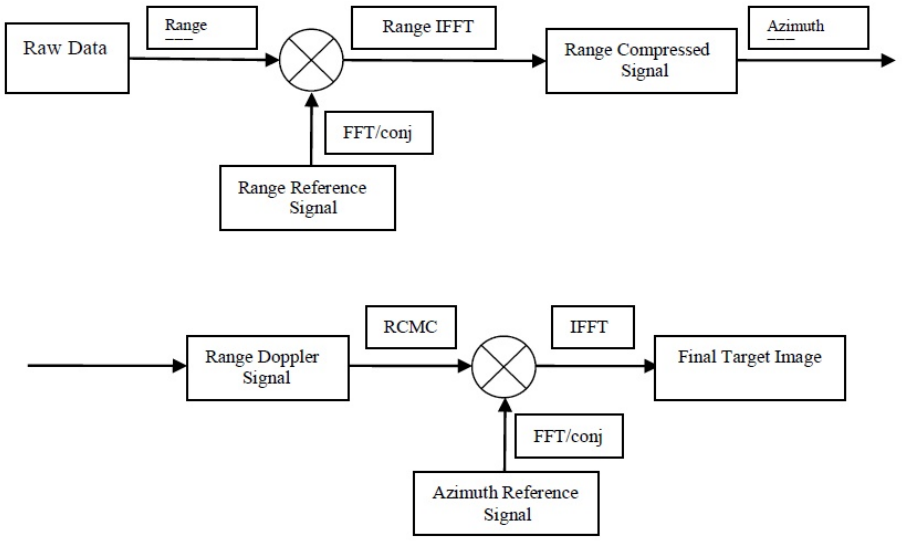

Figure 3.1: RDA Block Diagram

The block diagram for the Range Doppler algorithm is shown as Figure 3.1. The signals that are fed into the algorithm are the raw SAR signal space, Range Reference Signal, and Azimuth Reference Signal. The raw SAR signal space is the array of data which is captured by the radar platform as it traverses the target space. The Range and Azimuth Reference Signals are the ideal returns of a single point source. It is used as part of the matched filtering process. The operations involved in the process are FFTs, IFFTs, and multiplications of signals.

3.1.1 Range Compressed Signal

The first step in the algorithm is to compress the raw data in the range direction. This is done with a process called matched filtering. In the matched filtering process, a reference signal is compared with the incoming raw data to find the location where the received data matches a certain reference signal. In this context, the reference signal refers to the noiseless, ideal return signal of a theoretical point target. The matched filtering process is shown in Figure 3.2.

If the matched filtering is done in the time domain, the reference signal would be convolved with the complex conjugate of the received signal, and the peak location of the result would indicate where the raw SAR signal matched

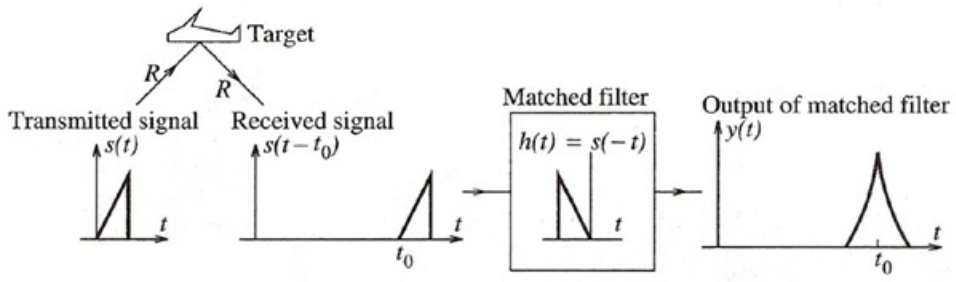

Figure 3.2: Radar Range Finding Matched Filter Example

the reference signal. In this Range Doppler implementation, a FFT is performed along each range bin of the raw SAR signal, as well as to the reference signal. This places both signals in the frequency domain. Once that is done, the match filtering is done with a simple multiplication of the raw SAR signal and reference signal. An inverse FFT is then performed along each range bin of the signal to bring it back to the time domain. The resulting signal is referred to as the Range Compressed signal[3].

3.1.2 Range Doppler Signal

The Range Doppler signal is obtained from the Range Compressed signal described in section 2.3.1. Once the Range Compressed signal is generated, a second set of FFTs are performed. This time, the FFTs are run with respect to the azimuth direction. The output of the transform will be in the time domain in the range direction, and the frequency domain in the azimuth direction. This signal is known as the Range Doppler signal, since the azimuth frequency, or Doppler frequency, is obtained.

The Range Cell Migration Correction (RCMC) is typically applied at this stage. The instantaneous slant range changes as the platform moves through the target space. Because of this, the target has a different Doppler frequency at different times throughout the simulation, and subsequently appears at multiple range bins in the Range Doppler signal. If the signal is compressed, the final image would show a washed out return instead of a point target. To correct for this, Range Cell Migration Correction is applied. The amount of shift, or migration, in meters can be calculated for each point on the Range Doppler signal by Equations 3.1 and 3.2.

$$R_{rd}(f_\eta) = \frac{R_{0_m}}{\sqrt{1 - \frac{c^2 f_\eta^2}{4V_r^2 f_0^2}}} \approx \frac{\lambda^2 R_{0_m} f_\eta^2}{8V_r^2} \tag{3.1}$$

$$f_\eta \approx -K_a \eta \approx \frac{2V_r^2 \eta}{\lambda R_{0_m}} \tag{3.2}$$

Since the Range Doppler signal data is quantized into discrete range and azimuth bins, the exact shift may not be able to be represented. Therefore, there will still be a slight blurring of the target in the final image.

3.1.3 Final Processed SAR Image

Once the RCMC has been applied to the Range Doppler signal, it is processed into the final image. Similar to the Range Compressed process, the signal is convolved with a reference azimuth signal using matched filtering. Since the Range Doppler signal is already in the frequency domain in the azimuth direction, it is simply multiplied with a reference azimuth signal in the frequency domain as well. The signal is then fed through an inverse FFT in the azimuth direction, resulting in the final target image[22, 14].

3.2 Two-Dimensional SAR Imaging through Simulation

The objective of this work is to explore two-dimensional target imaging methods.Two dimensional single point target is used in the simulation to understand how RDA is working. Parameters used for the simulation purpose is synthetic and used to improve Two dimensional SAR simulation. Simulation Results are based on Zaharris simulation and the simulation parameters and results are similar for a single point target.

FFT and IFFT is used for the simulation. First of all two dimensional signal space(in the form of array) is being calculated according to equation 2.4. It's result is shown in fig. 3.3 where cooler color represent the signal have low magnitude in that area and hotter color show that the signal intensity is very high. Adaptive Gaussian White Noise (AWGN) is also introduced to understand the impact on the signal space. Echo generated by SAR in entire azimuth

and center of range is clearly visible in simulation result.Echo energy that is spread over th azimuth is nothing but a sinc squared function which behave like decay pattern when the beam crossing the center (at lowest squint angle.). the above phenomena comes due to Doppler effect.Sinc squared function is not clearly visible As the duration of flight is very less i.e. only 3 second is used for the simulation purpose and hence squint angle will be nearly 0.859[22, 14].

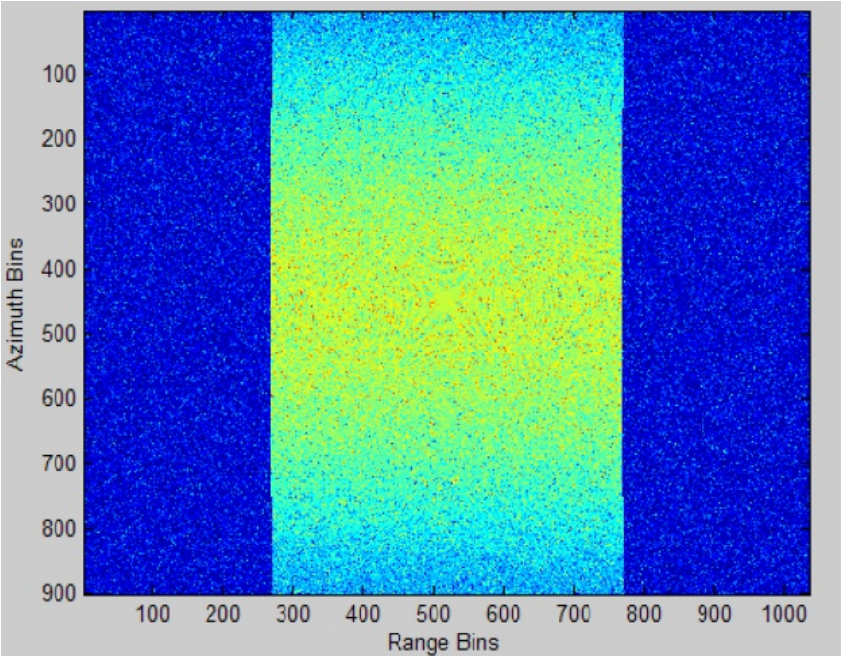

Figure 3.3: Raw SAR Signal Space

Fig.3.4 shows zoomed portion of center that come in fg. 3.3.High frequency sinusoidal components in both of the azimuth slow time(η) and range quick time (t) directions is being seen in the magnitude of the complex exponential term. Sinusoid frequency will increase as it is positive up chirp(refer equation 2.1).

The SAR signal space of Figure 3.3 is then put into the RDA as shown in Figure 2.6. First of all range reference signal in range frequency domain has to be assembled.In the simulation result of RDA, the upper left plot shows the reference signal magnitude in slow time (range time) domain and the upper right plot shows the range time phase of the reflected signal. The lower left plot is for the range frequency magnitude component and the lower right plot is for the range frequency phase component. The range cell migration is then calculated

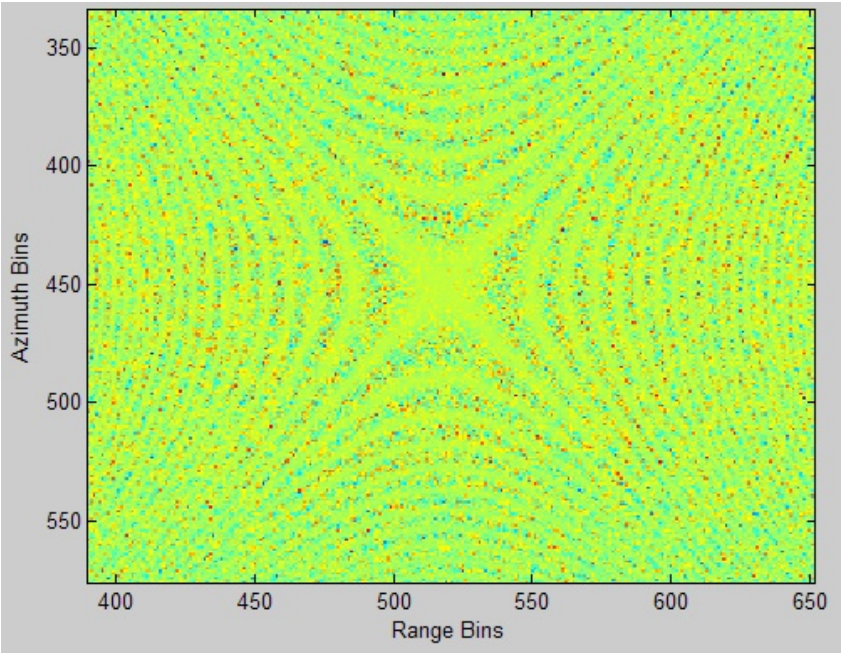

Figure 3.4: Zoomed in Center Raw SAR Signal Space

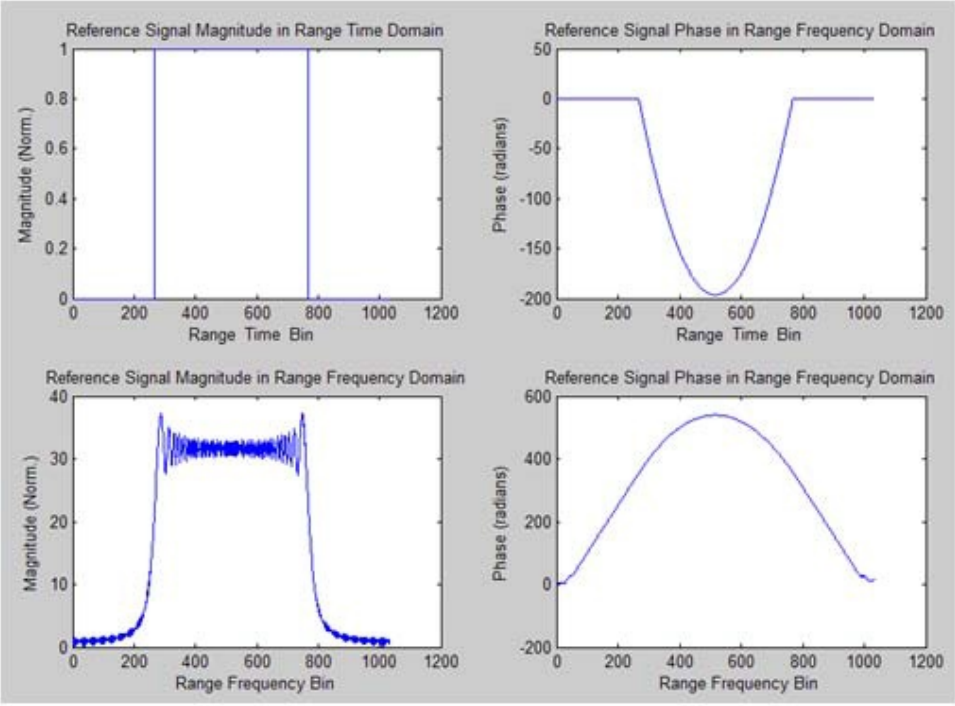

Figure 3.5: Range Reference Signal

after the range reference signal is obtained using approximation for low squint angle given by equation 3.1. A Fig. 3.5 below shows the simulation results obtained for the Equation 3.1. For the simulation purpose, it is rounded to the

nearest range cell as range migration can be corrected in discrete cells only. After range reference signal and RCM are obtained in the RDA , compression of the SAR signal space has to be done in the next step.

3.2.1 Range Cell Migration

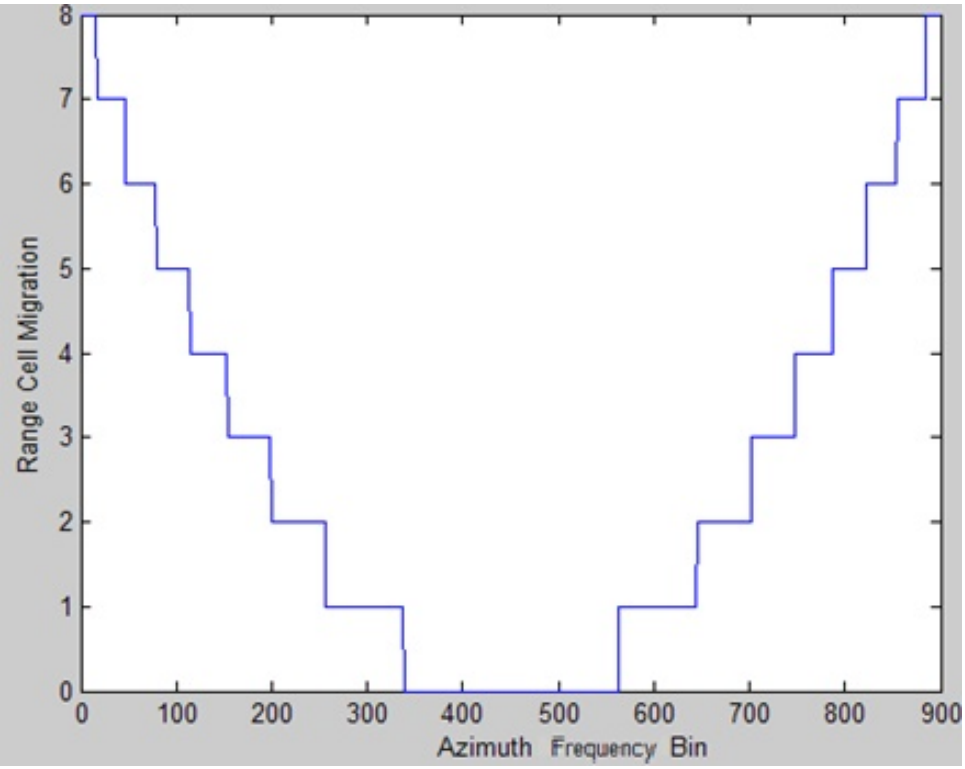

Figure 3.6: Range Cell Migration

As in the RDA block Diagram it is shown that the raw SAR signal is first fed into the RDA block and then taking Fast Fourier Transformation(FFT) in range time domain of raw SAR data. Pulse Repetition Frequency (PRF) for the simulation purpose is ,300 Hz, and times of the flight duration is ,3 seconds, so total 900 range time signals has to be processed in the simulation.
Range cell migration in this simulation is only valid when the target is within the regions of 400 and 500 bins of the azimuth. To deal with a target outside of this range, the RCM shift should be recalculated to center around the range of azimuth bins that are desired.
Next step is to take the FFT of each range time signal and add AWGN to each signal. Figure 3.7 shows in the upper left section the magnitude plot of an

example range time signal obtained halfway through the flight. Although this signal contains AWGN, it looks very similar to the reference range time signal shown in Figure 3.5 (above). The upper right section of Figure 3.7 shows the FFT of the center azimuth range time signal.

After taking the FFT of the range time signal, the next step is match filtering (or convolution) of the FFT of the time reversed range reference signal (shown in the lower left section of Figure 3.5) with the FFT of the range time signal (shown in the upper right section of Figure 3.7). The result of the matched filtering is shown in the lower left section of Figure 3.5.

The IFFT of the range matched filter output is then taken, resulting in a sharp and compressed pulse at the detected location of the reference signal, as shown in the lower right section of Figure 3.7. Although noisy backscatter can be seen in the image, this is negligible compared to the magnitude of the return from the target[14].

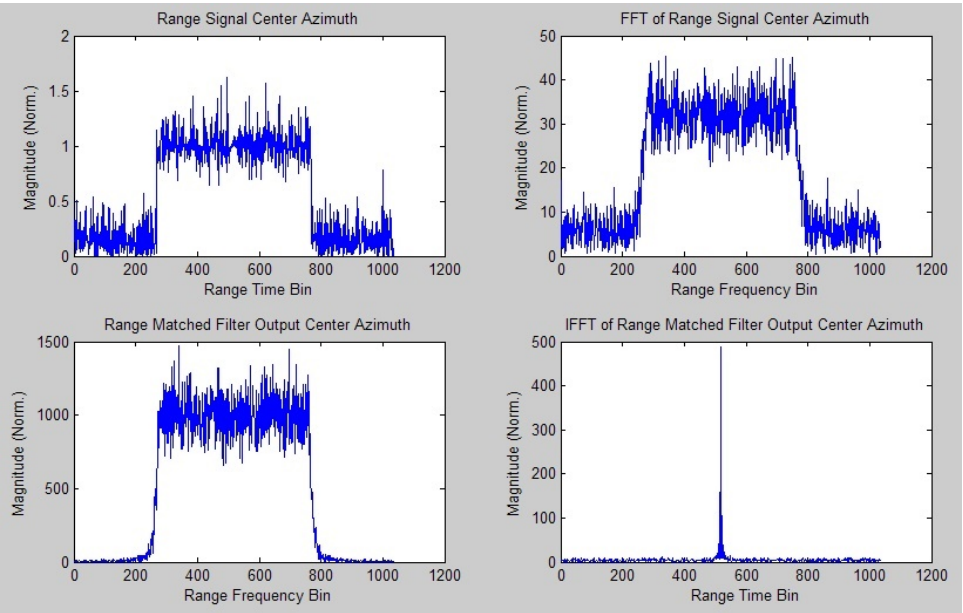

Figure 3.7: Range Time Signal at Center Azimuth Compression Example

The range compressed signal, once range compression is performed for each pulse, is shown in Figure 3.8.

The range cell migration that was predicted before the RDA filtering (shown in Figure 3.6) can be seen in Figure 3.8 (the image is zoomed-in in range to

example range time signal acquired halfway through the flight or the 450th signal acquired

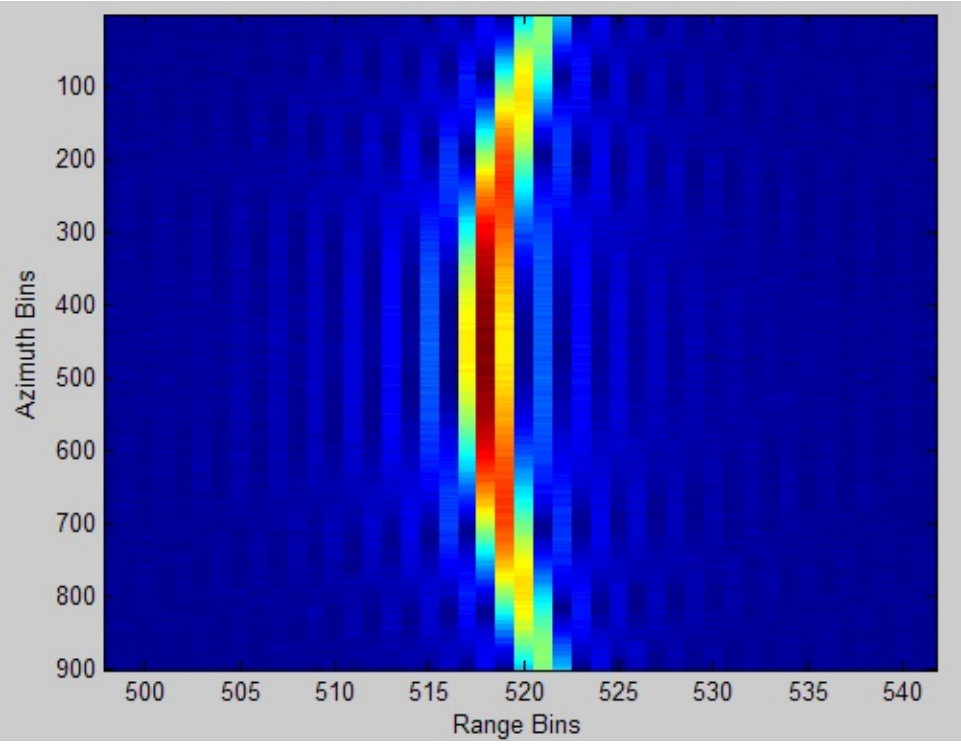

Figure 3.8: Range Compressed Image

emphasize the range cell migration). The next step in the range Doppler algorithm is to take the Fourier transform of the signal with respect to azimuth time. The main objective is to transform the azimuth time into the frequency domain while not affecting the range time. In this case, the Fourier transform is performed on each range bin. Figure 3.8 shows the result of taking Fourier transform on the center range bin, whereby the spectrum becomes a function of Doppler frequency (also called azimuth frequency). As depicted in Figure 3.8, at zero Doppler frequency the magnitude of the spectrum is the largest, which corresponds to the half-way point of the flight path. The result obtained from combining the Fourier transform of each range bin is shown in Figure 3.7. Range cell migration occurs in Figure 3.8 and thus it must be corrected in this domain[22, 14].

RCMC in the range-Doppler domain is performed before azimuth matched filtering. Figure 3.10 shows the image after RCMC is performed. The predicted shift shown in Figure 3.6 is used to shift the energy along the azimuth to counter cell migration in the range direction[22, 14].

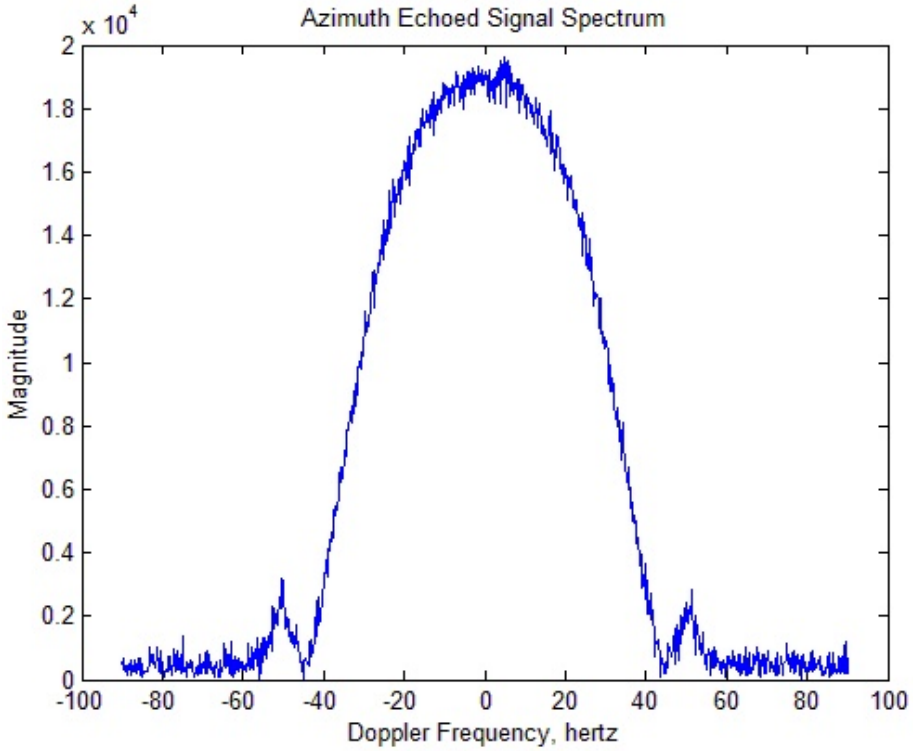

Figure 3.9: Image of range compressed signal

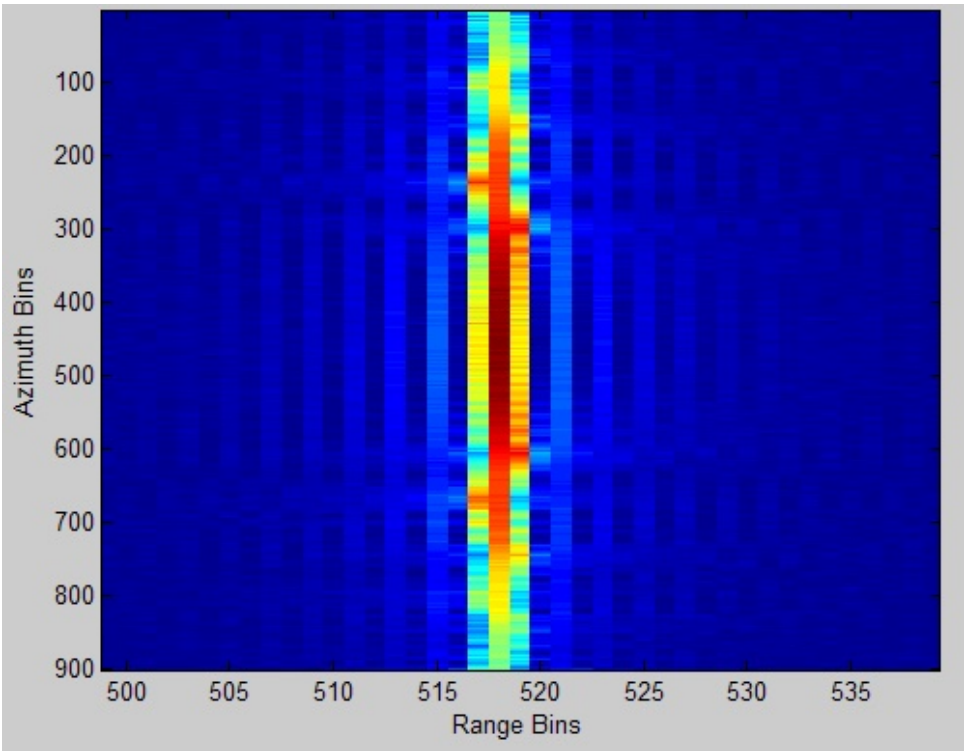

Figure 3.10: Image after RCMC

After RCMC is completed, the azimuth matched filtering process can be performed. The steps for azimuth matched filtering are similar to those used for the range matched filtering process. A reference signal in the azimuth direction is first defined. The main objective is to compress the azimuth portion of the signal while keeping the range portion unchanged. Since azimuth matched filtering is done in the frequency domain, the reference signal needs to be Fourier transformed. The reference signal and the azimuth data, both in the frequency domain, are then convolved. The final step is to take the inverse Fourier transform of the result obtained from the azimuth matched filtering. After azimuth compression is performed on all range bins in the footprint, the final target image can be constructed as shown in the Figure 3.11 (below)[22, 14].

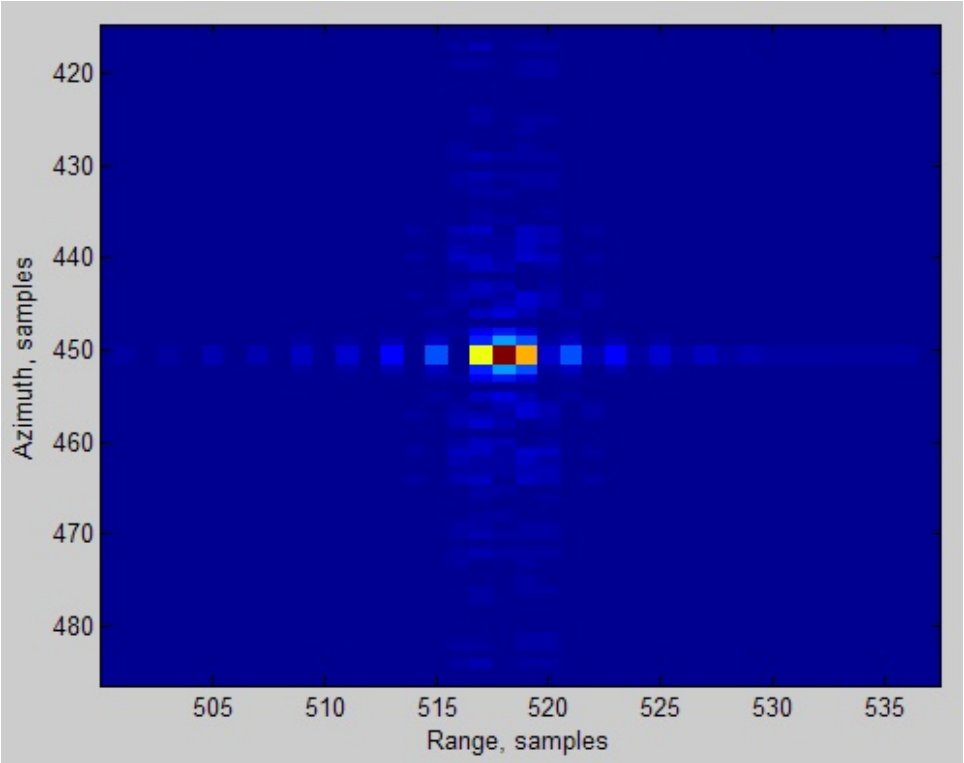

Figure 3.11: Final Processed SAR Image of Single Point Target

Chapter 4

The Keystone Transformation for Correcting Range Cell Migration

Introduction

Problem

Compensation by Range Shifting

The Keystone transformation

Chapter 4

The Keystone Transformation for Correcting Range Cell Migration

4.1 Introduction

Keystone Formating(KF)[10, 11] is a method that is capable of compensating multiple targets range migration without a prior knowledge of velocity of moving targets. Due to this reason it is widely used for imaging purpose for moving targets. In this thesis, slow time interpolation for keystone transformation is used. Consequently, the keystone interpolation process entails a small loss of slow-time support and therefore a small loss of Doppler resolution that increases[10].

4.2 Problem

Range-Doppler (RD) processing that collects a coherent processing interval (CPI) of slow-time/fast time data (*ft* and *st*) and performed a slow-time Discrete Fourier Transform (DFT) on all range bins is to convert it to an RD matrix. It is Implicit is the assuming that the target velocity v, CPI duration T_a, and range bin spacing δR are like that the targets range change within the CPI is less than one range bin, $vT_a < \delta R$. In other words, the target stays in the same range bin over the duration of the CPI. If this is the case, all of the target signature will be in the same range bin and a 1D slow-time DFT will result in a well-formed, full-resolution Doppler spectrum. For a constant-velocity target without slow-time

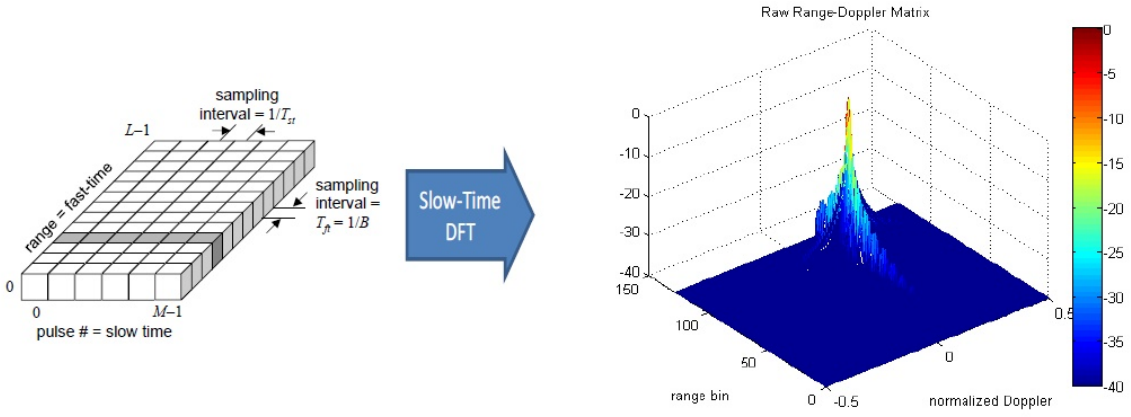

Figure 4.1: Range-Doppler matrix for a single target without range migration. Arrangement of fasttime/ slow-time data. Resulting range-Doppler matrix

windowing, this spectrum will be just a sinc function in the Doppler coordinate with a Rayleigh width of approximately $1/T_a$ Hz (assuming no windowing for sidelobe control). Figure 4.1 is a diagram of a notional data matrix in which the target stays in the same (gray-shaded) range bin over the CPI.

A simulated range-Doppler matrix was generated by modeling a target in range bin 100 that approaches the radar at 20 m/s. It is assumed that waveform and matched filtering used are such that the range response of the radar is an unwindowed sinc function with a Rayleigh resolution of $\Delta R = c/2B$ m. The radar frequency is $F_0 = 10$ GHz and its bandwidth is T_a= 200 MHz, giving ΔR = 0.75 m. However, the fast-time axis is oversampled by a factor of 2.3, so the spacing of the range bins is δR= 0.3261 m. The CPI is M = 101 pulses long at a PRF of 10 kHz, giving a CPI duration of = 10.1 ms. In this time, the target moves 0.202 m or 0.62 range bins. The target velocity corresponds to a Doppler shift of F_D= 13.33 kHz and an unaliased normalized Doppler shift of f_D = +0.133 cycles/sample. Note that the range- Doppler spectrum peak does occur at l = 100 and f_D = 0.133.

When the target does not remain within a single range bin over the CPI, range migration is said to occur. The target Doppler signature will smear in both range and Doppler. It smears in range because portions of the target signature appear in more than one range bin. It smears in Doppler because any one range bin contains the signature for only a portion of the CPI. Since Doppler

resolution (width of the a sinc mainlobe) in a given range bin is inversely proportional to signal duration in that range bin, the reduced duration degrades the Doppler resolution (broadens the mainlobe). Range migration is obviously more severe for fast-moving targets. However, it is also made worse in wide-bandwidth systems. Such systems have fine range resolution and therefore smaller spacing between range bins, so that a given amount of motion crosses more bins[6].

Consider an $L \times M$ ft/st matrix $y_{rd}[l,m]$. Suppose a radar transmits a series of $M = 2M_a + 1$ pulses which reflect from a target. The slow-time sampling interval (the radar PRI) is T_{st} seconds. Assume the slowtime span of the CPI is from $-T_a/2 = -M_a T_{st}$ to $+T_a/2 = +M_a T_{st}$, so that the center of the CPI is at time t = 0 and pulse M = 0. Note that the unambiguous Doppler range is $\pm 1/2T_{st}$ Hz.

If the fast-time sampling interval is T_{ft} seconds, the range bin spacing is $\delta R = c/2B$ meters. It is usually the case that $T_{ft} \simeq 1/B$, where B is the instantaneous bandwidth of the radar waveform; but we do not require this. Assume the range corresponding to the first range bin (l = 0) is R_0. Express the target range R_{ref} at the center of the CPI as $R_{ref} = R_0 + R_{rel}$, i.e. R_{rel} is the reference range relative to R_0. Let the range bin corresponding to R_{rel} be l_{rel}. Thus, $l_{rel} = (2R_{rel}/c)/T_{ft} = R_{rel}/\delta R$.

The target radial velocity relative to the radar is v m/s, with positive v representing approaching targets. The target range on the m^{th} pulse ($M_a < m < M_a$) will be $R_{ref} - vT_{st}m = R_0 + R_{rel} - vT_{st}m$, corresponding to range bin $l_{rel} - 2vT_{st}m/cT_{ft} = l_{rel} - 2vT_{st}m/\delta R$. (The range bin number is rounded to the nearest integer.)

Assume the RF is F_0 Hz. The radar transmits a pulse of the form $\bar{x}(t) = x(t)exp(j2\pi F_0 t)$, where $x(t)$ is the baseband waveform (for example, a simple pulse or LFM chirp, etc.). After taking out the delay of mT_{st} to the beginning of that pulses transmission and demodulation to baseband by multiplication with the function $exp(j2\pi F_0 t)$ to remove the carrier, the received fast-time signal for the m^{th} pulse will be of the form [11]

$$y_m(t) = \begin{array}{c} x\left(t-\frac{2}{c}\left(R_{ref}-vT_{st}m\right)\right)\exp\left[-j\frac{4\pi F_0}{c}\left(R_{ref}-vT_{st}m\right)\right] \\ x\left(t-\frac{2}{c}\left(R_{ref}-vT_{st}m\right)\right)\exp\left(-j\frac{4\pi F_0}{c}R_{ref}\right)\exp\left(+j\frac{4\pi F_0}{c}vT_{st}m\right)\end{array} \quad (4.1)$$

Amplitude factors are of no concern here and so have been ignored. Now assume this baseband signal is passed through the matched filter for the envelope x(t). Regardless of the particular waveform the matched filter output (after removing the matched filter delay) can be modeled as consisting of a dominant peak of Rayleigh width approximately 1/B seconds at the appropriate time delay, surrounded by low-amplitude sidelobes. For this analysis, a sinc function in fast time with a zero spacing of 1/B seconds, i.e. $x(t) = \sin(\pi Bt)/(\pi Bt) \equiv sinc(Bt)$, has been selected to represent a typical matched filter output

The demodulated and matched-filtered output becomes

$$y_m(t) = \exp\left(-j\frac{4\pi F_0}{c}R_{ref}\right)\exp\left(+j\frac{4\pi F_0}{c}vT_{st}m\right)\sin c\left(B\left(t-\frac{2}{c}\left(R_{rel}-vT_{st}m\right)\right)\right) \quad (4.2)$$

This analog data is converted to discrete fast-time data by sampling at the range bin interval of T_{ft} R_0, seconds. Sampling begins at the time delay corresponding to samples are taken at times$2R_0/c+l, l = 0,....,L-1$. The resulting fast-time vector is

$$y_m(l) \approx \begin{array}{c} \exp\left(-j\frac{4\pi F_0}{c}R_{ref}\right)\exp\left(+j\frac{4\pi F_0}{c}vT_{st}m\right)\sin c\left(B\left(T_{ft}l-\frac{2}{c}\left(R_{rel}-vT_{st}m\right)\right)\right) \\ \exp\left(\left(-j\frac{4\pi F_0}{c}R_{ref}\right)\right)\exp\left(\left(+j\frac{4\pi F_0}{c}vT_{st}m\right)\right)\sin c\left(BT_{ft}\left(l-\frac{2}{cT_{ft}}R_{rel}+\frac{2vT_{st}}{cT_{ft}}m\right)\right)\end{array} \quad (4.3)$$

The returns from each of the M pulses in the CPI are assembled into the raw fast-time/slow-time matrix $y_{rd}[l,m]$:

$$y_{rd}[l,m] = \exp\left(-j\frac{4\pi F_0}{c}R_{ref}\right)\exp\left(+j\frac{4\pi F_0}{c}vT_{st}m\right)\sin c\left(BT_{ft}\left(l-l_{rel}+l_m\right)\right) \quad (4.4)$$

Figure 4.1.b illustrates the pattern of data corresponding to Eq. (4.4) for the same case used in Fig. 4.1. Again, the simulation was carried out for L = 128 range bins and M = 101 pulses. The normalized Doppler shift is $f_D = F_D T_{st} =$

$(2vF_0/c)T_{st}$ = 0.133 cycles/sample. There is no significant range migration (0.62 range bins over the CPI) from the reference range bin of l_{rel} = 100 at the center of the CPI. Figure 4a shows the magnitude of the range bin vs. pulse number (fast time/slow time) data, illustrating that the signal peak stays within range bin (100). The oversampling factor of 2.3 in fast time makes it possible to see some of the sidelobe structure of the sinc response in fast time. Figure 4b shows the central portion of the resulting range-Doppler spectrum. The white dotted lines mark the reference range bin at the middle of the CPI (l_{rel} = 100) and normalized Doppler shift (F_D = 0.133) of the spectrum, and thus the expected spectrum peak location. The white square shows the expected Rayleigh resolution extent (expected location of first null) in each dimension. In the absence of range migration, the spectrum is a clean two dimensional sinc/asinc with its peak at the correct location and full resolution in both range and Doppler.

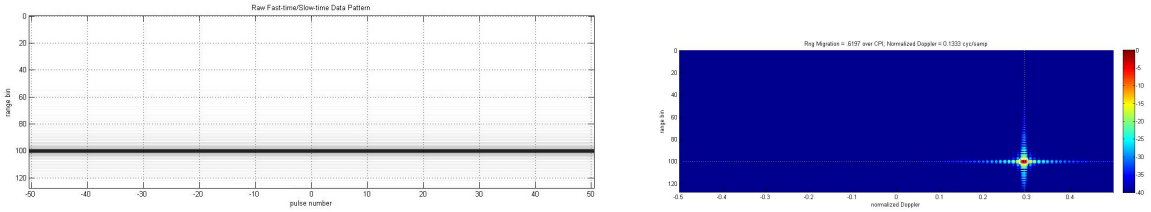

(a) (b)

Figure 4.2: Range-Doppler matrix with no range migration.(a)Range vs. pulse number. (b)Zoom into the central portion of the resulting range-Doppler matrix.

Figure 4.3 shows a similar example, with two changes. The target velocity is now 440 m/s, giving a significant range migration of 13.63 bins over the CPI. The RF frequency has been reduced to F_0 = 1 GHz, making the Doppler shift F_D = 2.933 kHz and the normalized Doppler frequency now F_D = 0.2933 cycles/sample. The reduction in F_0 allows for an unaliased Doppler at this velocity; see Section 6. It is clear that the signature is spread over a little more than 13 range bins and that its mainlobe in the Doppler dimension, while correctly centered, has also been severely broadened.

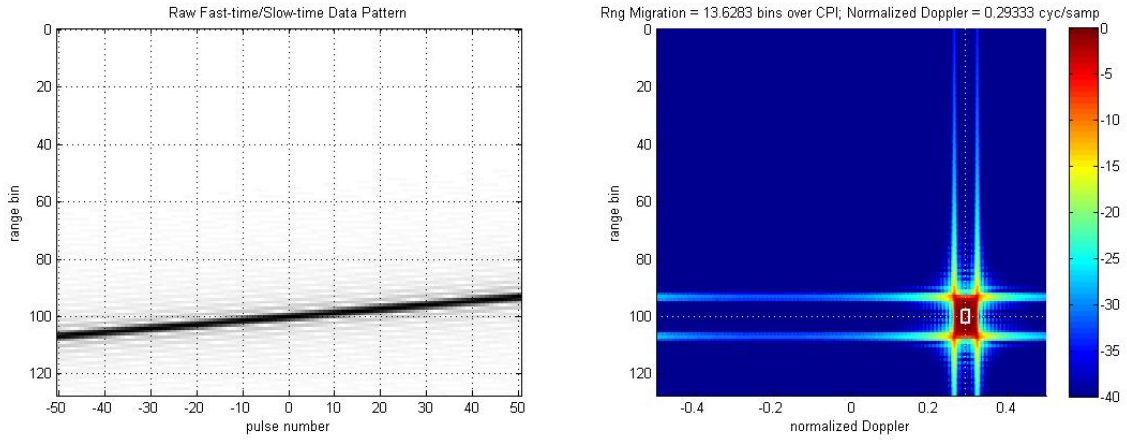

(a) (b)

Figure 4.3: Range-Doppler matrix with range migration(a)Range vs. pulse number.(b)Zoom into non-zero portion of the resulting range-Doppler matrix.

4.3 Compensation by Range Shifting

Goal of the keystone transformation is to develop a process that will compensate for the range migration so that the range-Doppler spectrum of the data in Fig. 4.3a looks like Fig. 4.2b instead of Fig. 4.3b. To begin, consider compensating for range migration in the not-very-useful case of a single target with known radial velocity. The target moves $vT_{st}/\delta R$ range bins closer to the radar on each successive pulse. This is easily corrected by shifting each successive fast-time vector by $-vT_{st}/\delta R$ bins with respect to the previous pulse data. The reference range to which all echoes will be shifted can be chosen arbitrarily. One obvious choice is the range R_{ref} (equivalently, R_{rel} relative to the first range bin at R_0) at the middle of the CPI.

The range can be shifted using properties of the discrete-time Fourier transform (DTFT). Recall that $y_m(l)$ is the fast-time data for the m^{th} pulse given in Eq. (3), and let $Y_m(\omega_l)$ be its DTFT. Then standard DTFT properties state that[11]

$$\mathbf{F}^{-1}\{\exp(-j\omega_l l_m)\, Y_m(\omega)\} = y_m[l-l_m] \equiv y'_m[l] \tag{4.5}$$

where $\mathbf{F}^{-1}\{\bullet\}$ represents the inverse DTFT (IDTFT). Because the desired shift $vT_{st}/\delta R = l_m$ is not integer in general, the quantity $y_m(l-l_m)$ means the corresponding shifted analog signal $y_m(t-(vT_{st}/\delta R)m)$ sampled at the times

$T_{ft}l$.

The shift is applied in practice by first computing the Kl-point DFT $y_m(k_l)$ of the fast time data, performing an fft shift operation to circularly shift the resulting vector of Kl DFT samples so that the sample corresponding to $kl = 0$ is in the center of the vector. The DFT size Kl must be greater than or equal to the number of range bins, L. The shifted DFT is then multiplied by the phase function of Eq. (4.5). The modified DFT is circularly rotated back to its original order, 4 and finally an inverse DFT is computed to obtain $y'_m(l)$. The inverse DFT returns a Kl-point fast-time sequence; only the first L points are retained.

Figure 4.4 illustrates the result of applying this compensation procedure to the data of Fig. 4.3a. The results are excellent: the target signature data is re-centered into range bin 100 for all pulses, resulting in a range-Doppler spectrum with the full expected resolution in both dimensions. The spectrum shape is nearly indistinguishable in shape from that of the negligible-migration case of Fig. 4.2, except for being centered at a different Doppler value in accordance with the change in velocity.

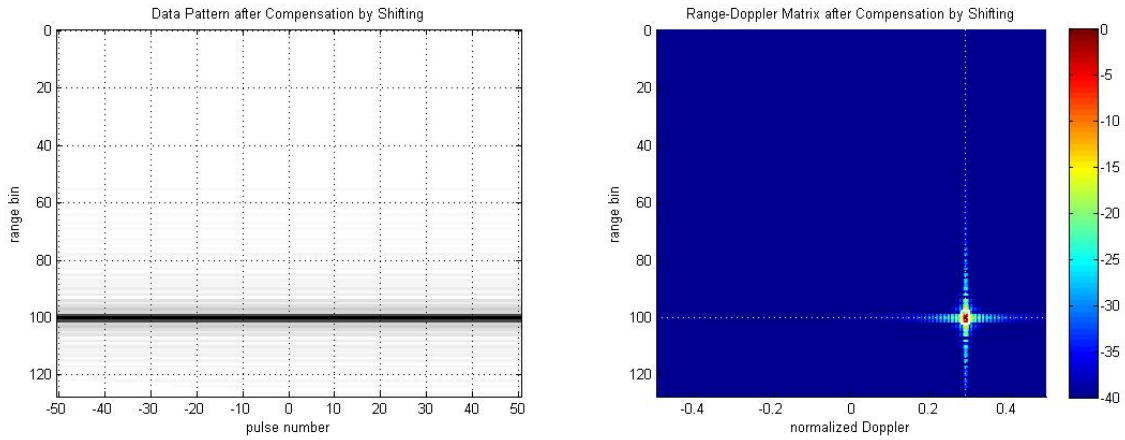

(a) (b)

Figure 4.4: Range-Doppler matrix with range migration and compensation using DFT phase multiplies. Compare to the spectrum shape in Figs. 2 and 3. (a) Range vs. pulse number.(b)Zoom into non-zero portion of the resulting range-Doppler matrix.

While the results in Fig. 4.4 are very good, they require two assumptions, both problematic:

1. The target velocity v is known. This is required to compute the DFT phase

modification function in Eq.(5). Knowledge of v implies that the target is already under track or that other sensors or information sources provide this information. Alternatively, the data can be processed with a series of different trial values of v in an attempt to identify the velocity by finding the value that best focuses the spectrum, usually interpreted as that value that provides the largest peak. if the target velocity might be aliased, it may also be necessary to estimate both the aliased velocity and the ambiguity number (number of foldovers);
2. There is only one target (or all targets have the same radial velocity). Otherwise, there is more than one value of v to be corrected, so there is no single DFT phase modification function that can be used.

Notice that if there were only a single target with a known velocity, the range migration could also be compensated by simply adjusting the start of the fast-time sampling times for each successive pulse so that the target remained at a constant delay relative to the transmission time for the current pulse.

4.4 The Keystone transformation

A more robust range migration compensation method can be developed as follows. First let us establish the goal, which is to obtain the range-Doppler spectrum of Fig. 4.4b corresponding to a target at relative range R_{ref} and normalized Doppler shift f_D, with full resolution in both dimensions as determined by the waveform bandwidth B and CPI duration (aperture time) T_a. It is convenient to work with continuous fast time t instead of sampled fast time l. In the fast time (range) dimension the desired response is, to within a complex constant, $sinc\left[B(t-2R_{rel}/c)\right]$. The fast-time Fourier transform (FT) of this function would have unit magnitude over the fast-time baseband frequency interval $F \in \left[-B/2, B/2\right]$ and zero elsewhere, and a phase of $exp\left[-j2\pi F(2R_{rel}/c)\right] = \exp\left(-j4\pi R_{rel}F/c\right)$ within that interval. This would be the same for each pulse (value of m) because there would be no range migration. In the cross-range dimension, the desired Doppler spectrum is the DTFT of a constant-frequency discrete-time sinusoid at the Doppler frequency $2vF_0/c$, sampled at the interval T_{st}. The corresponding slow-time phase progression is the se-

quence $exp\left[j2\pi(2vF_0/c)T_{st}m\right] = \exp\left(j4\pi vT_{st}(F_0/c)m\right)$. Combining the fast- and slow-time data patterns gives the ideal two-dimensional fast time/slow time data function.

$$y_{rd\_ideal}(t,m) = \exp\left(-j\frac{4\pi F_0}{c}R_{ref}\right)\exp\left(+j\frac{4\pi F_0}{c}vT_{st}m\right)\sin c\left(B\left(t-\frac{2}{c}R_{ref}\right)\right) \tag{4.6}$$

Now form the two-dimensional function $Y_{Rd\_ideal}(F,m)$ by computing the FT of $y_{rd\_ideal}(t,m)$ in fast time. The result will be

$$Y_{rd\_ideal}(F,m) = \begin{cases} \exp\left(-j\frac{4\pi}{c}(F+F_0)R_{ref}\right)\exp\left(+j\frac{4\pi}{c}F_0vT_{st}m\right), & \begin{matrix}-B/2 < F < +B/2 \\ -M_a < m < +M_a\end{matrix} \\ 0, \quad , \quad otherwise \end{cases} \tag{4.7}$$

Notice that the fast-time baseband frequency F and the velocity v are uncoupled, that is, they appear in separable terms. If the fast-time Fourier transform of the actual data $y_{rd}[t,m]$ can be manipulated to be in the form of Eq. 4.7, the corresponding range-Doppler spectrum will be correctly centered and well focused in both dimensions[11]

To that end, now consider the Fourier transform of the actual fast-time signal of Eq. (4.2). Using arguments similar to those leading to Eq. 4.7 gives

$$\begin{aligned} &\approx \exp(-j\tfrac{4\pi F_0}{c}R_{ref})\exp(+j\tfrac{4\pi F_0}{c}vT_{st}m)\exp\left[-j2\pi F\left(\tfrac{2}{c}\left(R_{ref}-vT_{st}m\right)\right)\right] \\ \mathbf{F}\{y_m(t)\} &= \exp\left(-j\tfrac{4\pi}{c}(F+F_0)R_{ref}\right)\exp\left(-j\tfrac{4\pi}{c}(F+F_0)vT_{st}m\right), \quad \begin{matrix}-B/2 < F < +B/2 \\ -M_a < m < +M_a\end{matrix} \\ &\equiv Y_{Rd}(F,m) \end{aligned} \tag{4.8}$$

Define a new slow-time variable that rescales the slow-time axis as a function of fast-time frequency according to

$$\tau' = \left(\frac{(F+F_0)}{F_0}\right)\tau \Rightarrow \ \tau \equiv \left(\frac{F_0}{(F+F_0)}\right)\tau' \tag{4.9}$$

At $F = 0$ the slow-time dimension is unchanged. For $F > 0$ it is expanded in slow time.

while for $F < 0$ it is contracted . For $F > 0$ this will have the effect of

stretching the sample-to-sample phase progression over a longer time interval, thus reducing the time rate of phase change and therefore the slow-time frequency. For $F < 0$ the slow-time frequency will be increased in the rescaled data.

Substituting from Eq. (4.10) for τ in Eq. (4.8) gives the new function

$$\begin{aligned} Y_{Rd\_key}(F,\tau') &\equiv Y_{Rd}\left(F,\left(\tfrac{F_0}{(F+F_0)}\right)/\tau'\right)\,\& \\ &= \exp\left(-j\tfrac{4\pi}{c}(F+F_0)R_{ref}\right)\exp\left(+j\tfrac{4\pi}{c}(F+F_0)v\left(\tfrac{F_0}{(F+F_0)}\right)\tau'\right) \\ &= \exp\left(-j\tfrac{4\pi}{c}(F+F_0)R_{ref}\right)\exp\left(+j\tfrac{4\pi}{c}vF_o\tau'\right) \\ &= Y_{rd\_ideal}(F,\tau') \end{aligned} \tag{4.10}$$

Equation (4.10) is the desired result. It shows that a fast-time FT and a slow-time rescaling according to Eq. (4.10) will result in a new function that is the fast-time FT/slow-time inverse FT of the desired range- Doppler spectrum. An inverse FT in the range dimension and a forward FT in the pulse number dimension will result in the focused range-Doppler image with no degradation in either range or Doppler due to range migration. The rescaling of Eq. (4.9) implies one-dimensional interpolation of the sampled slow-time data in each fast-time frequency bin. The interpolation factor varies with fast-time frequency. $T_{st}m$. An appropriate approach is bandlimited interpolation using sinc-based interpolation kernels [4], though simpler methods such as spline interpolation might be adequate in some cases. The region of support (ROS) of $Y_{Rd\_key}(F,\tau')$ in fast-time frequency is the same as that of the original data $Y_{Rd}(F,\tau)$, namely$\left[-B/2,B/2\right]$. The ROS in slow-time varies with fast-time frequency. The original slow-time variable τ is confined to the interval$-M_aT_{st} < m < +M_aT_{st}$. The range of the new slowtime variable $\tau'$is therefore

$$-\left(\frac{(F+F_0)}{F_0}\right)M_aT_{st} < \tau' < +\left(\frac{(F+F_0)}{F_0}\right)M_aT_{st} \tag{4.11}$$

The floor and ceiling functions are needed to restrict m to an integer range. For

$F < 0$ this range will be less than the original full range of $-M_a < m < +M_a$. For $F > 0$ Eq. (4.11) states that the range should be greater than $\pm M_a$. In practice, however, the range is limited to $\pm M_a$ because there is no data to support interpolation into a larger range.

Figure 4.5 illustrates the results of applying the keystone transformation to the same scenario used for Fig. 4.3. A Hamming-windowed bandlimited sinc interpolating filter was used to interpolate $Y_{Rd}[F,\tau]$in slow time. The filter length was 11 times the maximum of the slow-time sample spacing before and after interpolation. The specific value varies with fast-time frequency because of the variation in the interpolation factor $F_0/(F_0+F)$. Note in Fig. 5a that the range migration has been removed. The fading and fast-time smearing of the ft/st signature at the beginning and end of the CPI is due to end effects of the interpolation: the first and last few slow-time samples cannot be fully interpolated because the interpolation filter impulse response extends beyond the ends of the available data. This will result in a slight loss of Doppler resolution that will become more severe for longer interpolation filters. Figure 4.5b shows the resulting range-Doppler spectrum. The peak is correctly centered and obtains very nearly full resolution in both dimensions. Some modification of the sidelobe structure is evident in the X-shaped Doppler sidelobes, but this is of little consequence and can be reduced by windowing. A major advantage of the keystone transformation for range migration correction over the shifting process discussed earlier is that it correctly handles multiple targets. Notice that the rescaling of Eq.(4.10)

does not depend on target velocity v. Consequently, target velocity need not be known, and this process will simultaneously correct range migration for multiple targets of various velocities. Figure 4.6 illustrates this with another example using three targets having (reference range bin,velocity (m/s)) pairs of (30,200), (60,0), and (65,650). All radar parameters are unchanged. The resulting range migrations over the CPI are 6.1947, 0, and +20.1327 bins, while the normalized Doppler shifts are 0.1333, 0, and +0.4333 cycles/sample [11].

Figure 4.6 illustrates the results. Part (a) of the figure shows the ft/st data pattern. Note that two of the targets cross during the CPI. Figure 4.6b shows the range-Doppler spectrum before the keystone transformation. The zero-velocity

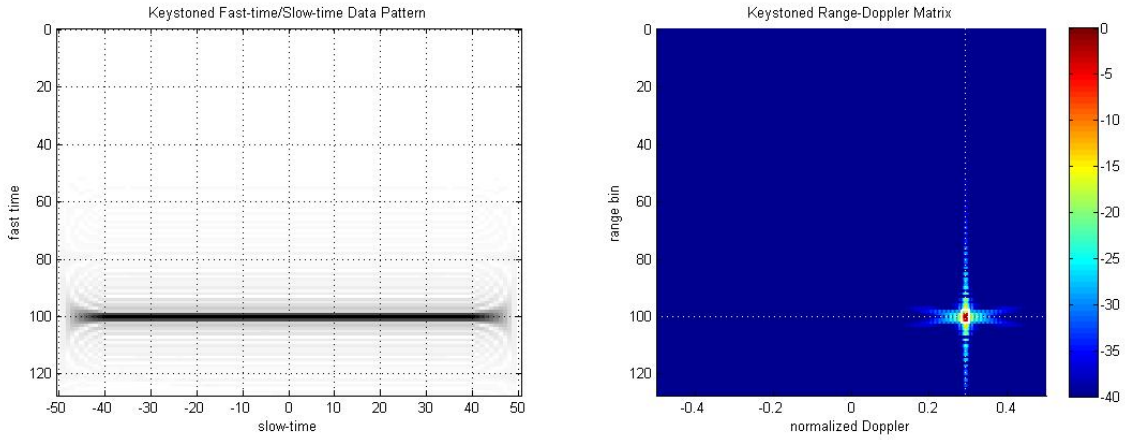

(a) (b)

Figure 4.5: Range-Doppler matrix with range migration and compensation using the keystone transformation. Compare to Figs. 4.3 and 4.4. (a) Range vs. pulse number. (b) Zoom into non-zero portion of the resulting range-Doppler matrix.

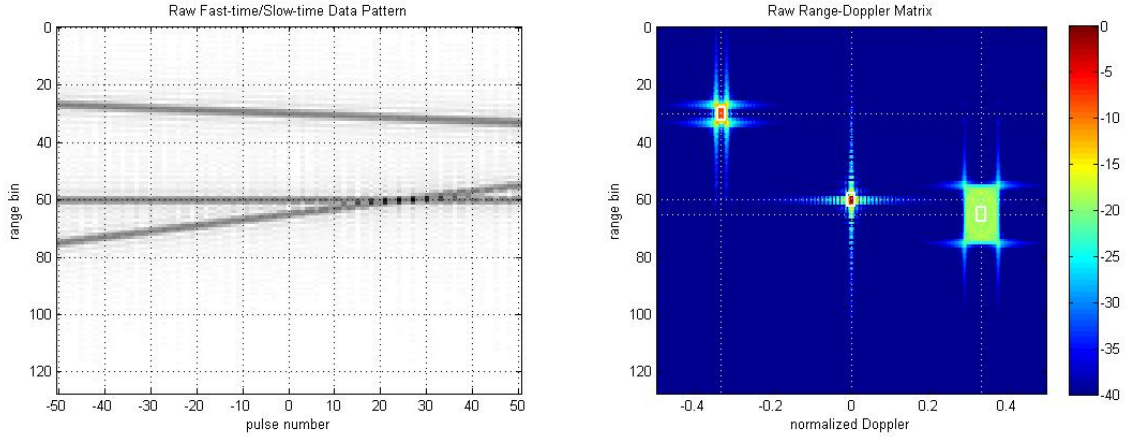

(a) (b)

Figure 4.6: Range-Doppler matrix with multiple targets at different velocities. (a) Range vs. pulse number. (b) Zoom into non-zero portion of the resulting range-Doppler matrix.

(non-migrating) target is well-focused; the other two are not, with the degree of defocus increasing at higher velocities (more range migration).

Figure 4.7 shows the results of applying the keystone transformation to this example. Figure 4.7a shows that each targets signature has been realigned to a single range bin. Figure 4.7b shows the resulting range- Doppler spectrum, now having nearly full resolution in both dimensions on all three targets, despite their differing velocities.

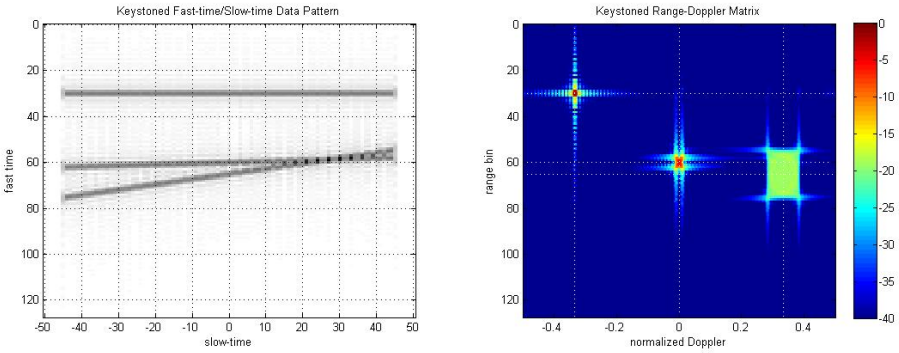

(a) (b)

Figure 4.7: Result of applying the keystone transformation to example of Fig. 6. (a) Range vs. pulse number. (b) Zoom into non-zero portion of the resulting range-Doppler matrix.

Chapter 5

Implimentation of Existing Methods in MATLAB

Simulation Results Obtained by RDA

Simulation Results Obtained on Correction of RCM using Keystone Transformation Method

Chapter 5

Implimentation of Existing Methods in MATLAB

5.1 Simulation results obtained by RDA

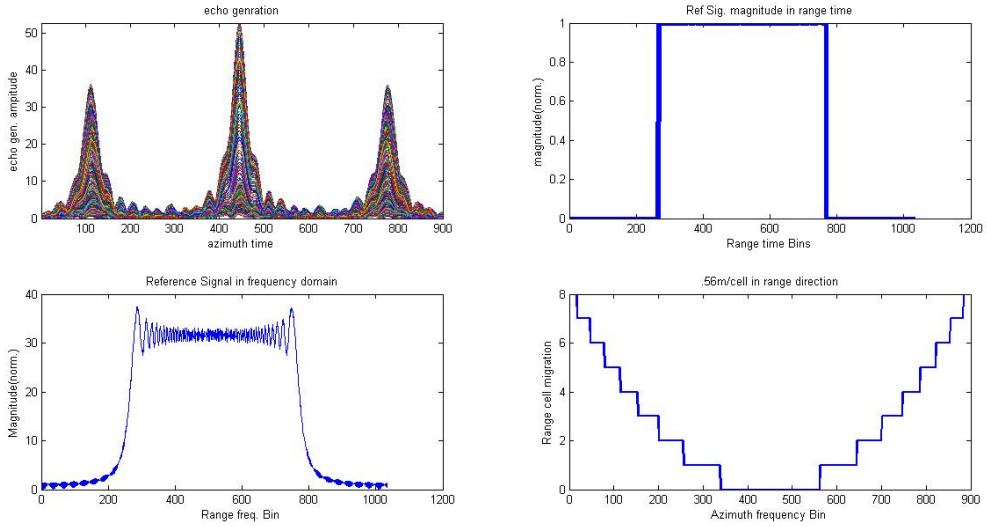

Figure 5.1: (a) Echo geenrated by targets. (b) Reference signal in range time domain. (c) Reference signal in frequency domain. (d) Range cell migration compensation output

Top most left corner of figure 5.1 shows echo received signal. clearly it is a sinc function. the top most right figure 5.1 shows reference signal magnitude in range domain.The bottom most left corner figure 5.1 in the simulation result shows band of frequency for the reference signal in fast frequency domain. The last figure shows how range cell migration correction is compensated to

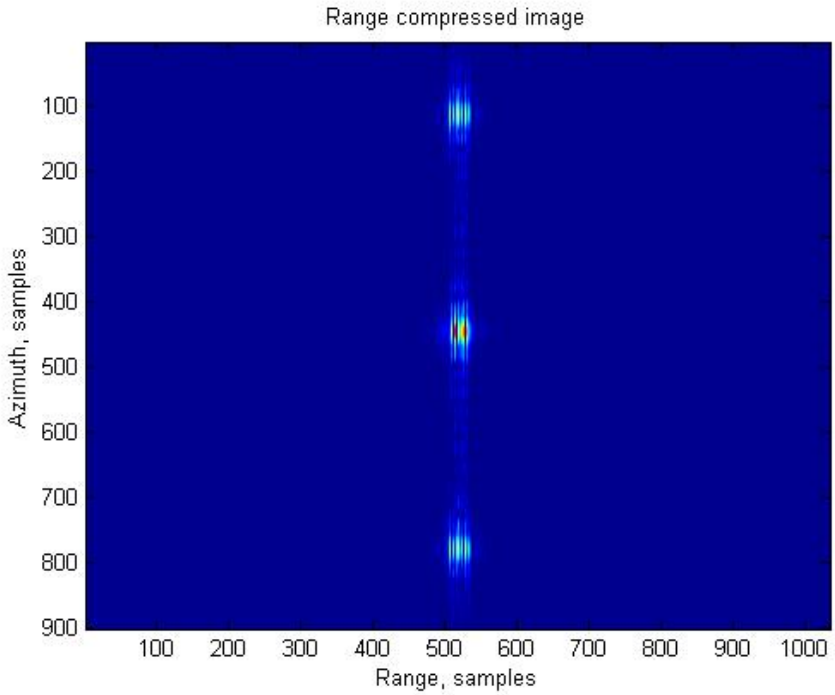

Figure 5.2: Range Compressed Image

the nearest range cell.

Figure 5.2 illustrate that the range compressed signal. In this figure image is compressed in range but need range cell migration. Hyperbolic curve for range compressed Image (caused by RCM) is not visible As squint angle is very low and flight duration of SAR is only 3 second for the simulation purpose.

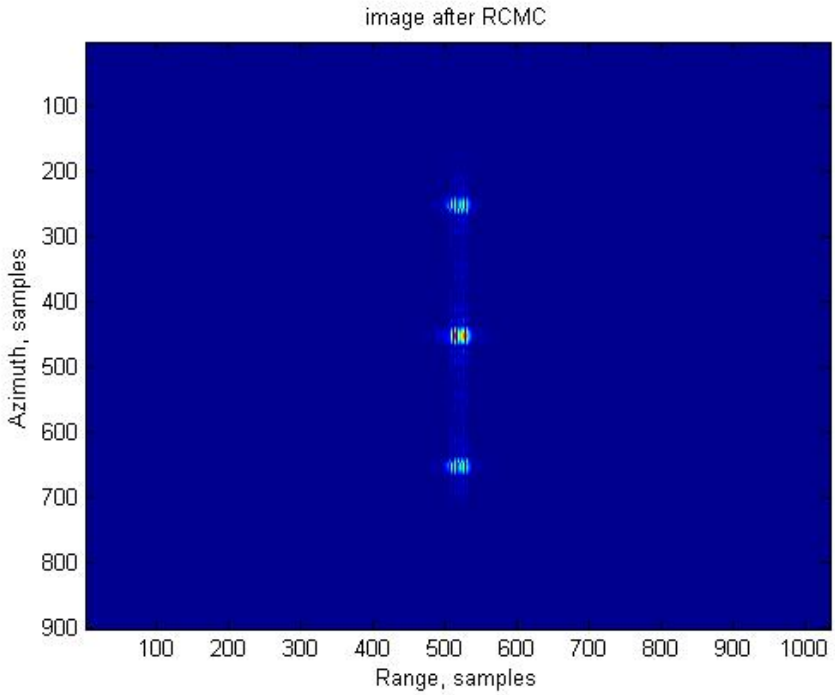

Figure 5.3: Image After RCMC

In figure 5.3, Range cell migration correction is performed in range doppler domain .The predicted shift shown in Figure 5.1 (above) is used to shift the energy along the azimuth to counter cell migration in the range direction.

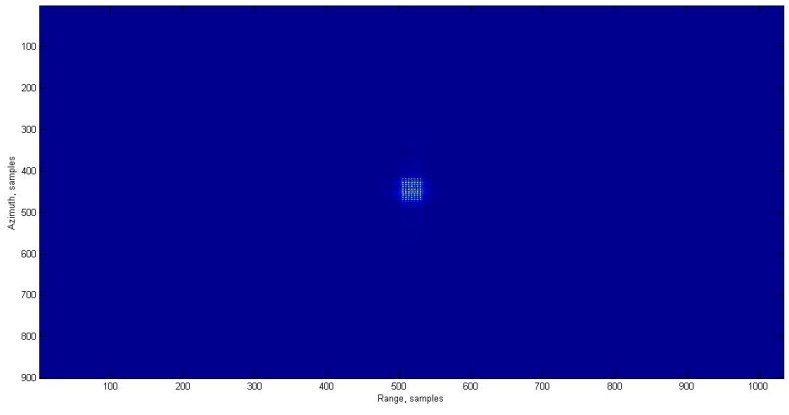

Figure 5.4: The final SAR image generated from the two dimensional simulation of a single point target

After azimuth compression is performed on all range bins in the footprint,

the final target image can be constructed as shown in the Figure 5.4

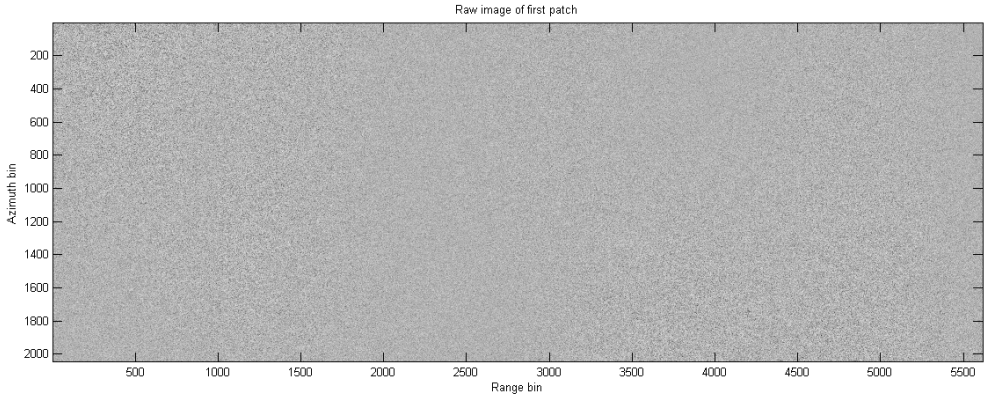

Figure 5.5: Raw Image

Range Doppler Algorithm implementation for SAR raw data shown in figure 5.5. Raw data is collected from ESA[13].

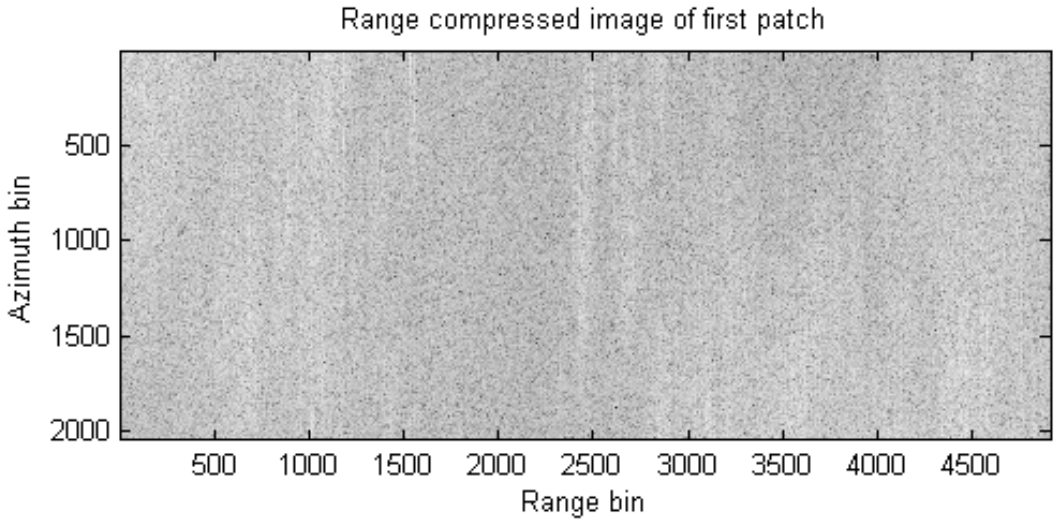

Figure 5.6: Range compressed image of first patch

Range compressed image after first patch is shown in figure 5.6. In this figure compression is done only in range. RCM has to be corrected after this.

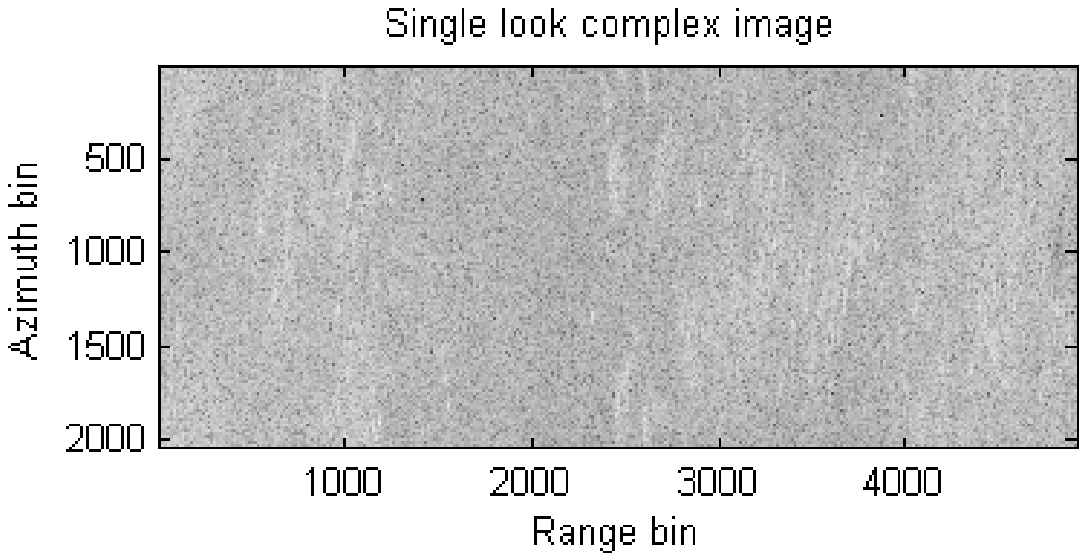

Figure 5.7: Single Look Complex Image

figure 5.7 shows Single Look Complex image after implementing range doppler algorithm[13].

5.2 Simulation Results Obtained On Correction of RCMC using Keystone Transformation Method

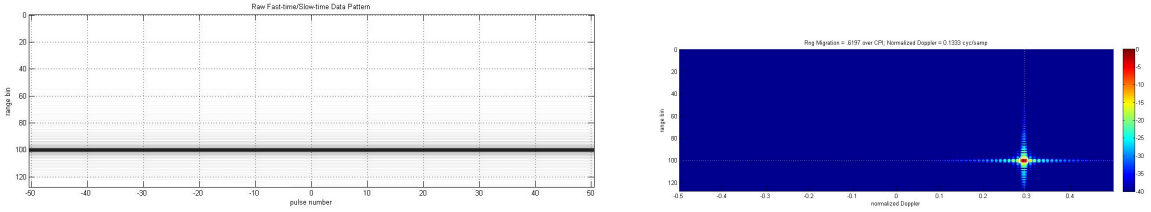

(a) (b)

Figure 5.8: Range-Doppler matrix with no range migration.(a)Range vs. pulse number. (b)Zoom into the central portion of the resulting range-Doppler matrix.

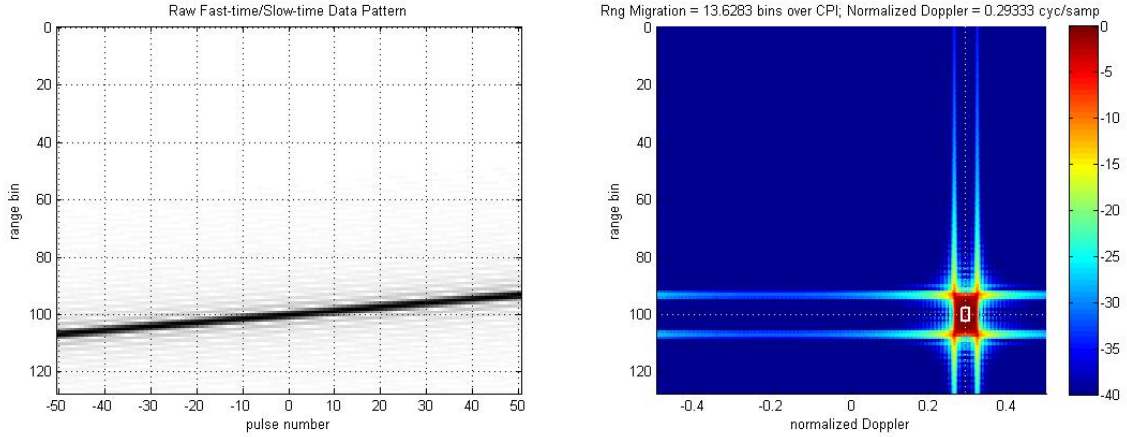

(a) (b)

Figure 5.9: Range-Doppler matrix with range migration(a)Range vs. pulse number.(b)Zoom into non-zero portion of the resulting range-Doppler matrix.

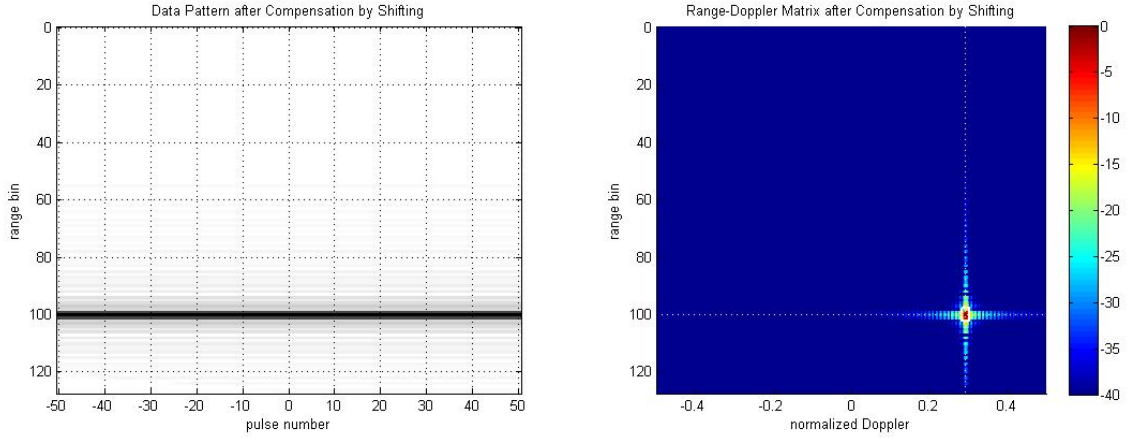

(a) (b)

Figure 5.10: Range-Doppler matrix with range migration and compensation using DFT phase multiplies. Compare to the spectrum shape in Figs. 2 and 3. (a) Range vs. pulse number.(b)Zoom into non-zero portion of the resulting range-Doppler matrix.

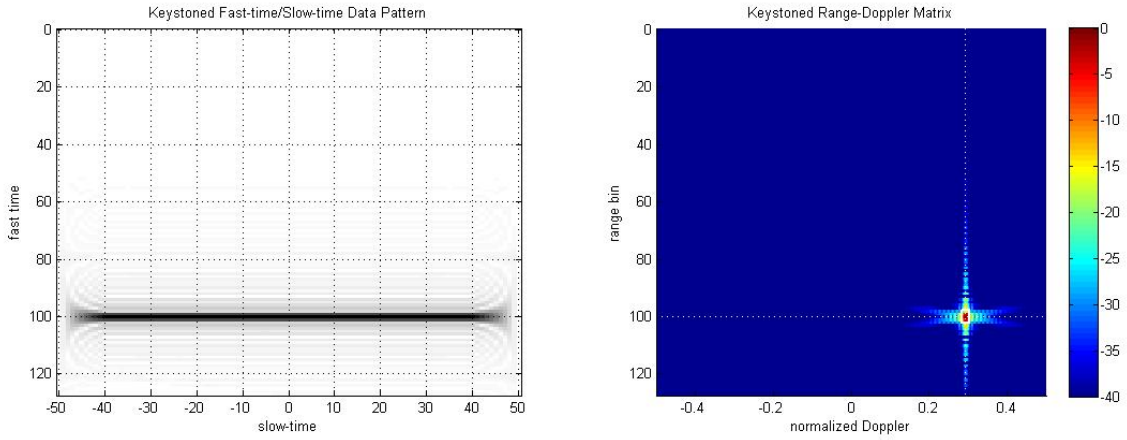

(a) (b)

Figure 5.11: Range-Doppler matrix with range migration and compensation using the keystone transformation. Compare to Figs. 3 and 4. (a) Range vs. pulse number. (b) Zoom into non-zero portion of the resulting range-Doppler matrix.

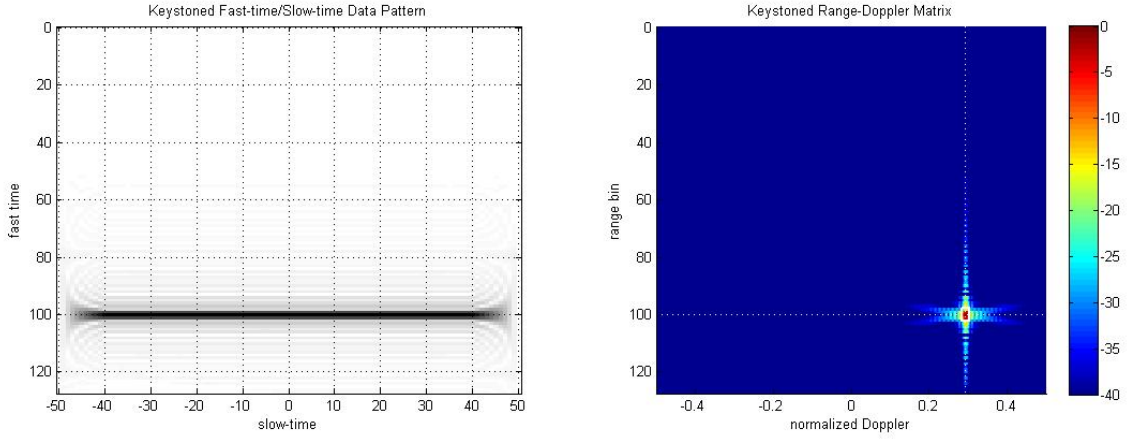

(a) (b)

Figure 5.12: Range-Doppler matrix with range migration and compensation using the keystone transformation. Compare to Figs. 3 and 4. (a) Range vs. pulse number. (b) Zoom into non-zero portion of the resulting range-Doppler matrix.

Chapter 6

Conclusion and Future Work

6.1 Conclusion

Range Doppler Algorithm is successfully implemented to form focused image. Here, we also compensate range migration problems occurred due to movement of SAR platform.

Keystone transformation technique is used for the correction of range cell migration. Here, it is observed that keystone transformation is more efficient than Range shifting methods for correcting range cell migration when velocity of target is not known by any other means. Here we found that how Range Doppler matrix varies without compensating range cell migration and get a smeared target in both range and doppler domain when relative velocity comes into picture.

6.2 Future work

Estimation of velocity of moving targets using Keystone Formatting without use of interpolation techniques.
Second-order keystone formatting for range curvature compensation, and range walk correction.

Bibliography

[1] Ashok Ambardar. *Digital Signal Processing-A Modern Introduction*. Thomson-Engineering, 2006.

[2] MJA Butler. *The application of remote sensing technology to marine fisheries: an introductory manual*. Number 295. Food & Agriculture Org., 1988.

[3] Ian G Cumming and Frank H Wong. Digital processing of synthetic aperture radar data: Algorithms and implementation (artech house remote sensing library). 2005.

[4] Richard J Doviak and Dusan S Zrnic. *Doppler Radar & Weather Observations*. Academic press, 2014.

[5] Li Jun, Liu Hong-Ming, He Zi-Shu, and Cheng Ting. Range migration compensation based on range-direction coupling in sfdlfm mimo radar. *WSEAS Transactions on Signal Processing*, 5(4):137–146, 2009.

[6] Robert J Marks. *Handbook of Fourier analysis & its applications*, volume 800. Oxford University Press London, 2009.

[7] Paul Ryan Mason. *MATLAB Simulation of Two-dimensional SAR Imaging by Range Doppler Algorithm: A Thesis*. PhD thesis, California Polytechnic State University, 2007.

[8] Alberto Moreira, Pau Prats-Iraola, Marwan Younis, Gerhard Krieger, Irena Hajnsek, and Konstantinos P Papathanassiou. A tutorial on synthetic aperture radar. *Geoscience and Remote Sensing Magazine, IEEE*, 1(1):6–43, 2013.

[9] Caner Ozdemir. *Inverse synthetic aperture radar imaging with MATLAB algorithms*, volume 210. John Wiley & Sons, 2012.

[10] Richard P Perry, Robert C DiPietro, and R Fante. Coherent integration with range migration using keystone formatting. In *Radar Conference, 2007 IEEE*, pages 863–868. IEEE, 2007.

[11] Mark A Richards. The keystone transformation for correcting range migration in range-doppler processing. *pulse*, 1000:1, 2014.

[12] TL Rusch, R Sankar, and JE Scharf. Signal processing methods for pulse oximetry. *Computers in biology and medicine*, 26(2):143–159, 1996.

[13] David Sandwell. SAR Image Formation Review of orbits Interferometry - correlated signals/geometry, 1999.

[14] Matthew Schlutz. Synthetic aperture radar imaging simulated in matlab. 2009.

[15] Cheuk Yu David So. *Synthetic Aperture Radar Rapid Detection of Range and Azimuth Velocities Implimented in MATLAB*. PhD thesis, California Polytechnic State University, San Luis Obispo, 2013.

[16] Mehrdad Soumekh. *Synthetic aperture radar signal processing*. New York: Wiley, 1999.

[17] Georger W Stimson. Airborne radar. *New Jersey: Scitech*, pages 317–322, 1998.

[18] Yue-Feng Tan, Zhu Xueyong, and Wen-Qin Wang. Impacts of velocity deviation on spaceborne high-resolution dpca sar. In *Computational Problem-Solving (ICCP), 2010 International Conference on*, pages 442–445. IEEE, 2010.

[19] Fawwaz Tayssir Ulaby and M Craig Dobson. Handbook of radar scattering statistics for terrain. *ARTECH HOUSE, 685 CANTON STREET, NORWOOD, MA 02062(USA), 1989, 500*, 1989.

[20] Michael A Wulder, Joanne C White, Richard A Fournier, Joan E Luther, and Steen Magnussen. Spatially explicit large area biomass estimation: three approaches using forest inventory and remotely sensed imagery in a gis. *Sensors*, 8(1):529–560, 2008.

[21] Chan-Su Yang, Youn-Seop Kim, and Kazuo Ouchi. Velocity estimation of moving targets on the sea surface by azimuth differentials of simulated-sar image. In *Geoscience and Remote Sensing Symposium, 2009 IEEE International, IGARSS 2009*, volume 3, pages III–809. IEEE, 2009.

[22] Brian Zaharris. *Two-dimensional synthetic aperture radar imaging and moving target tracking using the range doppler algorithm simulated in matlab: A thesis*. PhD thesis, California Polytechnic State University, 2007.

[23] Yongbo Zhao, Juan Wang, Lei Huang, and Rui Yang. Low complexity keystone transform without interpolation for dim moving target detection. In *Radar (Radar), 2011 IEEE CIE International Conference on*, volume 2, pages 1745–1748. IEEE, 2011.